공학박사학위논문

디사이클로펜타디엔 수지를 이용한 복합재료 액상성형공정 모델링 및 최적화

Modeling and Optimization of Liquid Composite Molding Process with Dicyclopentadiene Resin

2017 년 2 월

서울대학교 대학원

기계항공공학부

유 형 민

디사이클로펜타디엔 수지를 이용한 복합재료 액상성형공정 모델링 및 최적화

Modeling and Optimization of Liquid Composite Molding Process with Dicyclopentadiene Resin

지도교수 이 우 일

이 논문을 공학박사 학위논문으로 제출함

2016 년 11 월

서울대학교 대학원

기계항공공학부

유 형 민

유형민의 공학박사 학위논문을 인준함

2016 년 12 월

위 원 장 : 안 성 훈

부위원장 : 이 우 일

위 원 : 차 석 원

위 원 : 김 찬 중

위 원 : 김 한 상

Modeling and Optimization of Liquid Composite Molding Process with Dicyclopentadiene Resin

Hyeong Min Yoo
School of Mechanical and Aerospace Engineering
Seoul National University

Abstract

Demands for composite materials for civil applications in addition to military applications have been significantly increased. In the application for civil industries, it not only requires for a weight reduction but the efforts for achieving safety and a reduction of manufacturing cost has been sufficiently progressed. Dicyclopentadiene is a low viscosity resin which forms a poly-dicyclopentadiene rapidly through Ring opening metathesis polymerization (ROMP). This poly-dicyclopentadiene has outstanding properties of, low-temperature, water and impact resistances. Despite there are efforts for research developments of liquid molding technologies, dicyclopentadiene's unique curing behavior and an unstable reaction in an atmospheric

condition shows that the need for researches about an addition of reinforcements to the resin during the manufacturing process must be increased. The liquid molding apparatus which can be used with an addition of reinforcements was designed based upon the studies of the curing kinetics using the differential scanning calorimetry. Two different liquid molding methods have been developed depending on the resin viscosity, fiber volume fraction and the length. This apparatus was used for manufacturing samples where the mechanical properties were examined. Additionally, numerical analysis was performed in order to predict the manufacturing time depending on the resin's viscosity and the fiber volume fraction.

Keywords: Dicyclopentadiene, Fiber reinforced composites, Reaction injection molding (RIM), Differential scanning calorimetry (DSC)

Student Number: 2012-22559

Table of contents

List of Figures

List of Tables

Chapter 1

INTRODUCTION

1. Introduction

1.1. Overview and problem description

The application and demands for composite materials have been increasing for automotive industries in addition to military and aerospace applications. In the use of composite materials for automotive applications critically requires to lower the manufacturing cost which sufficiently maintaining safety and crashworthiness. Thus using the resin with a superior impact resistance would be favorable. The resin must be studied and the researches on processing of composite material must be undertaken.

Dicyclopentadiene (DCPD) is a colorless liquid with a low viscosity extracted from crude oil. When activated by a catalyst, the DCPD resin rapidly undergoes a ring opening metathesis polymerization (ROMP) reaction to form the network structure of polydicyclopentadiene (p-DCPD). Tungsten (W), molybdenum (Mo), ruthenium (Ru), and chromium (Cr) are commonly used catalysts for making p-DCPD through ROMP. Among these catalysts, W, Mo based catalyst are widely used because of their good mechanical properties and cheap price. However, the reaction is unstable in the atmosphere and the viscosity is relatively high according to the addition of the activator to activate the reaction. On the other hand, Ru-based catalysts have been favored recently

because of their capability of carrying out the polymerization reaction in the air (1-4). The reaction mechanism of the DCPD resin with the Ru based Grubbs catalyst is illustrated in Figure 1. As can be seen, the molecular weight increases as the double bond of the norbornene is ring-opened by the Ru catalyst. Upon the ring-opening, the double bond of cyclopentene is also ring-opened where the cross-linking begins (5-7). The p-DCPD with network structures has good mechanical properties at a significantly low temperature, water resistance, and impact resistances. These properties are advantageous in applications to automobile bumpers, heavy machinery, and offshore structures (Figure 2) (6, 8, 9). However, there are less desirable attributes related to its unfavorable smell and unstable reactions, and these and other problems have stymied progress and redirected focus to DCPD composite reinforcements. At the same time, the low viscosity and short reaction time of DCPD make it especially useful for reaction injection molding (RIM) (9, 10). Figure 3 describes the RIM manufacturing process where the resin and catalyst are mixed in a mixing head prior to mold injection using a relatively low pressure (11). For the RIM technology capable of adding reinforcements, there are two ways, Reinforced reaction injection molding (R-RIM) and Structural reaction injection molding (S-RIM). R-RIM uses current two liquid bi-component with injection of the resin into the mold with an addition of reinforcements as shown in figure 4. On the other hand, S-RIM generally uses a fiber mesh which is firstly arranged in the mold before the polymer mixture injection takes place (12). These preforms are impregnated by the resin

injected through the injection nozzle of the mold. After the mold is filled, the resin is cured and the product is removed from the mold (Figure 5). Since the mold filling time takes few seconds to minutes, it is possible to manufacture long fiber reinforced composites rapidly. Numerous researches for optimizing the process parameters have been performed (13, 14).

RIM requires the resin and the catalyst to be mixed thoroughly in order for the reaction to be correctly triggered and completed. However, it can be very difficult to obtain a high quality defect-free product since it requires not only precise mixing times and optimal curing temperature profile but also a vacuum process for removing voids.

1.2. Literature review

The production of p-DCPD with the reaction triggered by Mo, W based catalyst have been manufactured and used without any specific reinforcements due to its high impact resistance property. Due to the unstable reaction under atmospheric conditions and a high viscosity results the use of Ru based catalyst despite the expensive cost. The Ru based DCPD resin has a rapid reactivity resulting a fast curing speed. This resulted sufficient researches based on self-healing applications had been undertaken as shown in figure 6. The examples of researches is specifically based on the types of catalysts (15), the concentration of catalysts (2), the degree of recrystallization (16) and the studies of the

interface between the fiber and the matrix (8, 17, 18) as shown in figure 7 to 10.

1.3. Research objective and scope

In this study, the characterization of the resin must take place in prior to manufacture the composite materials. Using the DSC, the total heat of reaction under the isothermal condition was obtained. The change of total heat of reaction and the reaction peak for different temperatures, the optimum molding temperature and the operating time was obtained. Based on these values, a lab scale S-RIM system was designed to facilitate the addition of reinforcements along with the catalyst and resin mixing during p-DCPD composite fabrication. Rigorous air-free nitrogen atmospheres and ventilation systems were employed for the processing of the p-DCPD composites.

Additionally, a surface treatment was used to increase the adhesion between the glass fibers and the DCPD. Ultimately, the effect of the norbornene-treated glass fiber reinforcements was evaluated and high quality fiber reinforced p-DCPD composites were manufactured. Additionally, a numerical analysis for S-RIM was undertaken for various resin viscosities and fiber volume fractions in order to correctly predict the molding time.

Chapter 2

EXPERIMENT

2. Experiment

2.1. Materials

RIMTEC provided two different resins with one composed with the W based catalyst and the other with the Mo based catalyst. Where on the other hand, the neat DCPD resin and Ru-based Grubbs 2nd catalyst were purchased from the Sigma-Aldrich Corporation (Korea) (Figure 11, 12). A chopped strand mat intertwined with a glass fiber with average diameters of 16 μm and lengths of 50 mm was purchased from Owens Corning Corporation. The carbon fabric used in this experiment was from the Muhan composite with the model code C-120. Figure 13 shows the used glass fiber strand mat and the carbon fabric. Norbornene-based silane for surface treatment was provided by Gelest Corporation.

2.2. Characterization of DCPD resin

2.2.1. Properties of DCPD monomer

The specification of the Mo, W and Ru based catalyst are shown in figure 14. Even though the densities are similar, resins with Mo and W has higher viscosities in

comparison to the Ru based DCPD resin since it contains an activator for a catalyst activation.

2.2.2. Differential scanning calorimetry analysis

The curing behavior of DCPD was investigated with DSC (TA instrument, Q20) (Figure 15). DSC recorded the heat flow in accordance with the time under the isothermal conditions ranging from 45 to 100 °C. When the measurement of the DCPD resin is undertaken at isothermal conditions, it is difficult to obtain the reaction peaks since the curing reaction advances considerably during the time for the DSC pan to reach the desired temperature (2). In order to avoid the problem, the part of the pre-mixed catalyst and the DCPD solution (2wt.%) cooled in a liquid nitrogen was used for DSC measurements in order to delay the DCPD reaction (Figure 16). The total heat of reaction of the ROMP process was estimated from the DSC reaction peak plots using the following equation:

$$\text{Total heat of reaction , } H_{total} = \int_0^{t_f} \frac{dq}{dt} dt \qquad (1)$$

Where q is the heat flow, t_f is the end point of reaction.

2.2.3. Three-point bending test

In order to confirm the fact that the DCPD resin possessed a lower degree of cure at a lower temperature, the p-DCPD specimen was made under different mold temperatures. According to ASTM D790, three point bending tests were conducted with a universal testing machine (UTM, LLOYD instrument, LR50K, UK).

2.3. Processing of fiber reinforced composites

2.3.1. Reinforcement reaction injection molding (R-RIM) process

First, filling two of the three DCPD solutions where excluding the solution which would be used for the fiber dispersion in the enclosed vessels for the defoamation. Then, reinforcement and the solution for the dispersion in the enclosed vessel for dispersion and defoamation was filled (Figure 17). The three vessels with three different DCPD solutions were connected by using teflon tubes. Following the connection, a vacuum condition for defoamation was made by using a vacuum pump. In an enclosed vessel for defoamation and the dispersion vessel, a stirrer was operated alongside defoamation.

After the end of a defoamation, we inject two solutions which are contained in an enclosed vessel for a defoamation into the enclosed vessel for defoamation and dispersion. After the injection, stirrer had to be operated continuously to disperse the reinforcement. Furthermore, a vacuum condition was maintain. Once the mixing was completed, the vacuum pump was turned off and the nitrogen gas was injected into the enclosed vessel for a defoamation and dispersion in order to maintain 1 atm condition. By using the pressure, the mixed resin was injected into the mold. Before undertaking this step a vacuum condition in the mold was made to remove any excess air. In the injection step, since the total volume of DCPD resin is bigger than the volume of mold, the resin trap between mold and vacuum pump was set which created a vacuum condition in the mold. After the end of injection, heating tape was operated until the curing process was over. The specimen using this manufacturing method actually showed that it had 24% higher tensile strength than that of the specimen manufactured using the open mold technology as shown in table 3.

2.3.2. Structural reaction injection molding (S-RIM) process

The S-RIM equipment was designed to manufacture the fiber (fabric, mat etc.) reinforced DCPD composite specimens with dimensions of 150 x 120 x 3 mm^3. The

customized S-RIM equipment shown in Figure 18 was specifically designed to minimize voids by pulling vacuum. The equipment facilitated mixing of the DCPD resin and the catalyst prior to injection into the mold with a preformed chopped glass strand mat or carbon fabric. The resin vessel was wrapped with heating tape to maintain a temperature of 40°C since the melting point of the DCPD resin is 33°C. The mold itself was also maintained at 40°C with a temperature controller. A vacuum pump was connected to the resin vessel to remove the void within the vessel. After removing the void, the catalyst was injected into the resin vessel from the top and stirred solution was injected into the mold. The composite specimens were made with a mold temperature which was increased up to 100℃. The manufactured specimens were cut and tested according to the ASTM standards of D638-10 for the tensile strength, D790-10 for the flexural strength, and D256 for the impact strength. 5 specimens were tested at each test (Figure 19).

2.3.3. Norbornene based silane treatment

In order to increase the interfacial adhesion between the DCPD resin and the fiber, previous treatment was stripped away and the surface of the fibers were treated with norbornene based silanes (8, 19) (Figure 20). The silane treatment was performed after

drying the glass fiber at 200°C for 24 hours to remove moisture and impurities from the surface. The specific surface treatment solution was a mixture of silane, ehanol, and acetic acid mixed in a 5:4:1 mass ratio. The treatment solution was added to the glass fibers in a 100:1 mass ratio. The treated glass fibers were used after further drying for 4 hours at 140℃ (18).

2.4. Results and discussion

2.4.1. DSC and Three-point bending test results

DSC scans were performed for the DCPD resin in order to accurately establish the composite molding temperature and the mixing time (Figure 21). Initially, the endothermic peak was observed when the frozen DCPD and catalyst mixture melted. Separately, the exothermic peak was observed when the polymerization began. The polymerization was complete within 2 min. Higher reaction temperatures resulted in shorter polymerization times and narrower peaks. The total heat of reaction was obtained by measuring peak areas for each temperature (Figure 22). When the polymerization occurred at higher temperature, it showed that the total heat of reaction was also high.

For temperatures above 80°C, the total heat of reaction converged to 330 J/g. This is thought to be due to insufficient cross linking of DCPD under 80°C. Additional DCPD specimens were prepared at 45, 60, and 100°C and subjected to bending tests in order to verify if insufficient polymerization had occurred at lower temperatures.

Figure 23 and Table 1 shows that the specimens have different mechanical properties depending on the molding temperature. Further, p-DCPD specimens prepared at lower temperatures had low maximum bending stress and modulus values. These data support the notion that the polymerization did not fully occur at temperatures below 80°C. As such, the minimum experimental temperature for DCPD resin was determined to be 80°C.

2.4.2. Curing kinetics of DCPD resin

Differential Scanning Calorimetry (DSC) was used to model the curing behavior. As it can be seen in figure 24, different isothermal test data was curve fitted using the thermoset resin's Autocatalytic model shown in table 2.

2.4.3. Mechanical properties of DCPD composites

In prior to manufacturing the specimen with an addition of reinforcements, the mechanical properties for different catalysts were examined. As it can be seen in Figure 25, specimens with W and Ru based catalysts showed higher tensile strength. Additionally, p-DCPD with the W based catalyst had the highest impact resistance hence it can be said that the specimen with the W-based catalyst outstands the mechanical properties of them all (Table 4).

2.4.3.1. Molybdenum (W) based catalyst

The tungsten catalyst with the highest mechanical properties of the neat, specimens with an addition of the milled glass fiber was manufactured. With increasing the fiber content, the untreated showed a reduction of the mechanical properties while the treated showed a small increase in both tensile and bending strengths with the impact resistance reduced Figure 26.

2.4.3.2. Molybdenum (Mo) based catalyst

The use the Mo based catalyst enables to add higher glass fiber volume fraction in comparison to the use of the W-based catalyst. Similarly, all of the mechanical properties for the untreated reduced for increasing the fiber volume fraction while the treated

showed a marginal increase of the tensile and bending strengths with the impact resistance reduced as shown in Figure 27.

2.4.3.3. Tungsten (W) and molybdenum (Mo) mixture based catalyst

In order to supplement the drawbacks of the w-based catalyst and the Mo-based catalyst, the W-based catalyst was mixed with the Mo-based catalyst. The concentration of the W-based catalyst was varied and the tensile properties are shown in Figure 28. With the mixing of the two catalysts resulted increased mechanical properties and the 25wt% of the W-based catalyst was found to be the optimum value for obtaining the highest tensile strength. This was due to the fact that the cl ion of the tungsten catalyst accelerated the secondary ring opening metathesis. (Figure 29, 30). Despite the lower impact strength in comparison to the W-based catalyst while resulting a higher tensile strength, specimens with 25wt% were manufactured and the mechanical properties were examined as shown in Figure 31. The specimens were manufactured with a long glass chopped fiber (4mm) since it was found that adding milled fiber had no effect. As it can be seen in Figure 32, the tensile and the bending strength increased by 11% and 41% respectively which the impact strength reduced by 36%.

2.4.3.4. Ruthenium (Ru) based catalyst

Results from the previous experiment showed that the tensile and the bending strength increased while the impact strength reduced. This was mainly due to insufficient length and the volume fraction of the chopped fiber (Figure 33 and 34). Therefore, laying preform sheets with long fibers in prior to injecting the resin and the catalyst was considered as an alternative. As it can be seen in Figure 35, if the composite part was molded using the catalysts (W, Mo, W+Mo), the mixture began to cure during injection due to its high viscosity. Therefore, S-RIM process was undertaken by using the Ruthenium based catalyst. Since the viscosity was sufficiently low, full impregnation of the fibers was achieved despite the high fiber volume fraction as shown in Figure 36.

Specimens for fiber volume fractions 25, 40 and 55wt% were made and their mechanical properties were examined and presented in Figure 37 and table 5. Higher quantities of glass fibers resulted in increased tensile, flexural, and impact strengths. With glass fiber contents of 25, 40, 55wt.%, tensile strength increased by 50, 76, 101%, flexural strength by 51, 85, 93%, and impact strength by 248, 508, 767% , respectively, compared with the neat p-DCPD. Enhanced mechanical properties of GF/p-DCPD can be explained by achieving sufficient impregnation despite the short processing time even at the highest loading levels.

As it can be seen in Figure 38, 55wt% CF/p-DCPD composites were made and the

maximum shear stress and shear modulus were measured and presented in Figure 39 and table 6. The values of the shear stress and shear modulus were 50MPa and 1.3GPa respectively. Additionally, in order to examine the DCPD composite's impact strength, CF/p-DCPD was compared with CF/Epoxy as shown in Figure 40. Despite the same fiber volume fraction, CF/p-DCPD have shown impact strength 3 times greater than the CF/Epoxy.

Chapter 3

NUMERICAL ANALYSIS

3. Numerical analysis

3.1. Solution algorithms

3.1.1. Governing equations

Conservation of mass :

$$\nabla \cdot \mathbf{u} = 0$$

$$\frac{\partial u_i}{\partial x_i} = 0$$

Conservation of momentum :

$$\rho\left(\frac{\partial \boldsymbol{u}}{\partial t} + \boldsymbol{u} \cdot \nabla \boldsymbol{u}\right) = \nabla \cdot \sigma + \rho S$$

$$\rho\left(\frac{\partial \boldsymbol{u_i}}{\partial t} + u_j u_{i,j}\right) = \nabla \cdot \sigma_{ij} + \rho S_i$$

Constitutive equations :

$$\boldsymbol{\sigma} = \boldsymbol{\tau} - p\mathbf{I}$$

$$\boldsymbol{\tau} = 2u_f\mathbf{D}$$

$$\mathbf{D} = \frac{1}{2}[(\nabla \boldsymbol{u}) + (\nabla \boldsymbol{u})^T]$$

$$\sigma_{ij} = \tau_{ij} - p\delta_{ij}$$

$$\tau_{ij} = 2u_f D_{ij}$$

$$D_{ij} = \frac{1}{2}\left(\frac{\partial u_i}{\partial x_j} + \frac{\partial u_j}{\partial x_i}\right)$$

Where **u**, ρ, σ, S, $\boldsymbol{\tau}$, p and D are the velocity vector, the density, the total stress tensor, the body forces, the viscous stress tensor, the pressure and the rate of deformation tensor, respectively.

Boundary conditions for velocity :

$$u_i = \hat{u}_i \qquad \text{on } \Gamma_u \ (essential\ boundary\ condition)$$

$$t_i \equiv \sigma_{ij} n_j = \hat{t}_i \quad \text{on } \Gamma_t \ \text{(traction boundary condition)}$$

where Γ_u and Γ_t are mutually complementary subsets of the boundary Γ. $\hat{\mathbf{u}}$, $\hat{\mathbf{t}}$, $\hat{\mathbf{n}}$ denotes the velocity vector prescribed on Γ_u, the traction vector prescribed on Γ_t and the unit vector normal to Γ_t, respectively.

Energy conservation equation :

$$\rho C_p \left(\frac{\partial T}{\partial t} + u \cdot \nabla T \right) = \nabla \cdot (\mathrm{k} \nabla \mathrm{T}) + \mathrm{Q} + \Phi_t$$

$$\rho C_p \left(\frac{\partial T}{\partial t} + u_i T_{,i} \right) = (\mathrm{k} T_{,i})_{,i} + \mathrm{Q} + \Phi_t$$

where T is the temperature, C_p is the specific heat, k, Q and Φ_t are thermal conductivity, the rate of internal heat generation and the viscous dissipation in the fluid, respectively.

Boundary conditions for temperature :

$$T = \hat{T} \qquad \text{on} \qquad \Gamma_T$$

$$\mathbf{q} = k\frac{\partial T}{\partial \boldsymbol{n}} = h(T - T_\infty) \text{ or } q_n = (kT_{,i})n_i = h(T - T_\infty) \qquad \text{on} \qquad \Gamma_q$$

where **q** denotes the heat flux normal to the boundary Γ_q. h represents the convection heat transfer coefficient and T_∞ is the temperature in the free stream at the outer edge of boundaries. Γ_T and Γ_q are mutually complementary subsets of the boundary Γ.

The initial condition in given for the whole domain Ω as follows:

$$u_i(0,x_i)=u_{i0}$$

$$T(0,x_i)=T_0$$

Where it is required that

$$n_i u_{i0}=n_i \hat{u}_i \quad \text{on } \Gamma_u$$

$$(u_{i0})_{,i}=0 \quad \text{in } \Omega$$

In order that a solution exists. If Γ_t is null, the boundary condition for velocity must satisfy the following global condition for t≥0.

$$\oint_{\Gamma} n_i \hat{u}_i dS = 0$$

u_{i0} and T_0 are the initial value for velocity and temperature, respectively(20-22).

3.1.2. Porous media flow

The flow behavior of typical liquid can be described with the Navier-Stokes equation for incompressible flow given in the following form :

$$\rho \frac{Du}{Dt} = -\nabla p + \mu \nabla^2 u$$

Where ρ is the density of the liquid and μ is the viscosity, p is the pressure and u is the velocity vector. For low Reynolds number flows, stokes approximation is available and the non-linear momentum terms are neglected.

$$0 = -\nabla p + \mu \nabla^2 u$$

The most generally accepted equation to describe the porous media flow for Newtonian fluid is Darcy's law as follows (23, 24).

$$Q=-\frac{K}{\mu}A\frac{\Delta p}{L}$$

Where Q is the flow rate, A is the normal cross-sectional area, ∇p, μ, K are the pressure gradient, the viscosity of the fluid and the permeability tensor of the medium.

In fluid filling process simulation of porous media flow, the governing equation is following:

$$u=-\frac{K}{\mu}\Delta P$$

$$\nabla \cdot u=0$$

$$\nabla \cdot \left(-\frac{K}{\mu}\nabla P\right)=0$$

where u is the volume-average Darcy velocity and sectional area, p is the pore-average fluid pressure.

3.2. Modeling and conditions

The S-RIM process modeling was performed and shown in Figure 41. The curing kinetics and viscosity variation of the resin with temperature was analyzed and flow simulation was carried out using these analyzed results. Before resin was cured, the viscosity change of resin with temperature was expressed using the exponential viscosity model (Figure 42). The domain of the porous media made of a fibrous preform was designed similarly to a real fibrous media (Figure 43). The porosity was determined using the volume fraction and the reference values of the permeability of the air and the resin were used as shown in Figure 44.

3.3. Results of numerical simulation

3.3.1. Viscosity

For resin's viscosities of 0.4, 0.1 and 0.04 pa·s, the flow of the mixture into the mold with the time variation is presented in Figure 45 to 47. By looking at the graph showing the filling ratio dependent on the process time, it clearly shows that over 99% of the resin successfully filled the mold for the resin's viscosity between 0.04 to 0.1 pa·s. On the

other hand, for the resin's viscosity of 0.4 pa·s, it showed that not even 75% filling was achieved within 30 seconds (Figure 48). From this analysis, it can be concluded that for the high viscosity resins (W, Mo Catalysts), it is unsuitable for the S-RIM process. Whereas the low viscosity resin below 100 pa·s (Ru based) was found to be suitable for the S-RIM process.

3.3.2. Fiber volume fraction

Numerical analysis was performed for different fiber volume fractions. It was found that for the highest volume fraction of 38%, the flow filling time was successfully within 30 seconds (Figure 49, 50).

3.3.3. Mold temperature

The flow analysis was carried out with mold temperature using the calculated exponential viscosity model. As it can be seen from the Figure 51, the higher the mold temperature, the shorter the process time. However, when the mold is filled, the resin have a higher temperature distribution as the mold temperature rises (Figure 52). When the mold temperature is too high, the quality of the product is poor because the resin is

cured rapidly at a temperature above 80℃. Therefore, it is necessary to set an optimal process temperature.

Chapter 4

SUMMARY AND CONCLUSION

4. Summary and conclusion

The total heat of reaction and the curing time were obtained through the DSC analysis of the DCPD resin. The total heat of reaction increased with increasing temperature before plateauing at 80°C. Further, lower maximum strength and modulus values were measured with the three point bending tests for specimens prepared at lower curing temperatures. These data mean the notion that the curing did not fully at temperature below 80℃. Hence, the experimental apparatus was designed to operate for curing temperatures above 80°C with stirring times of less than 30 s. Also a vacuum process was adopted in order to remove any unwanted voids within the mold.

Fiber reinforced DCPD composites were manufactured using R-RIM process and its mechanical properties were examined. In order to supplement the drawbacks of the existing resin, Mo, W mixed catalysts were used in order to increase the resin's strength. DCPD composites made using this resin had increased the tensile and the flexural strengths whereas the impact strength reduced due to the short length of the fibers. This led to the use of long fibers hence implementing the S-RIM process. By having to correctly examining the filling aspect depending on the resin's viscosity and different fiber volume fractions, a composite part with a high fiber volume fraction was made using the resin with Ru-based catalyst. Furthermore, the S-RIM process was used to

manufacture carbon fabric added p-DCPD composite. The shear property was carefully examined and it was found that the impact strength was much greater than that of made with the epoxy resin.

Use of flow simulation and optimized condition of S-RIM process enabled the fabrication long fiber reinforced composite specimens with up to 55 wt.% fiber content. The corresponding test results revealed increases in tensile, flexural, and impact strengths depending on the increase in the fiber content. Due to the low viscosity of Ru based DCPD, fibers could be sufficiently impregnated with the resin well despite the large fiber volume fraction. These data imply that this new DCPD composite manufacturing approach as a promising route to stronger, lighter, and more efficient structures.

References

1. Schwab P, Grubbs RH, Ziller JW. Synthesis and Applications of RuCl2(CHR‘)(PR3)2: The Influence of the Alkylidene Moiety on Metathesis Activity. Journal of the American Chemical Society. 1996;118(1):100-10.

2. Kessler MR, White SR. Cure kinetics of the ring-opening metathesis polymerization of dicyclopentadiene. Journal of Polymer Science Part A: Polymer Chemistry. 2002;40(14):2373-83.

3. Li H, Wang Z, He B. Ring-opening metathesis polymerization of dicyclopentadiene by tungsten catalysts supported on polystyrene. Journal of Molecular Catalysis A: Chemical. 1999;147(1):83-8.

4. Brown EN, White SR, Sottos NR. Microcapsule induced toughening in a self-healing polymer composite. Journal of Materials Science. 2004;39(5):1703-10.

5. Davidson T, Wagener K. The polymerization of dicyclopentadiene: an investigation of mechanism. Journal of Molecular Catalysis A: Chemical. 1998;133(1):67-74.

6. Yang Y-S, Lafontaine E, Mortaigne B. Curing study of dicyclopentadiene resin and effect of elastomer on its polymer network. Polymer. 1997;38(5):1121-30.

7. Sheng X, Lee JK, Kessler MR. Influence of cross-link density on the properties of ROMP thermosets. Polymer. 2009;50(5):1264-9.

8. Jeong W, Kessler MR. Toughness Enhancement in ROMP Functionalized Carbon Nanotube/Polydicyclopentadiene Composites. Chemistry of Materials. 2008;20(22):7060-8.

9. Macosko CW. RIM Fundamentals of Reaction Iniection Molding. 1989.

10. Lee LJ, Ottino JM, Ranz WE, Macosko CW. Impingement mixing in reaction injection molding. Polymer Engineering & Science. 1980;20(13):868-74.

11. Kim DH, Kim SC. Vitrification effect during the reaction injection molding (RIM) process of epoxy resin. Polymer Engineering & Science. 1989;29(7):456-62.

12. Ashida K. Polyurethane and related foams: chemistry and technology: CRC press; 2006.

13. Chang W, Kikuchi N. Analysis of non-isothermal mold filling process in resin transfer molding (RTM) and structural reaction injection molding (SRIM). Computational Mechanics. 1995;16(1):22-35.

14. González-Romero V, Macosko C. Process parameters estimation for structural reaction injection molding and resin transfer molding. Polymer Engineering & Science. 1990;30(3):142-6.

15. Yang G, Lee JK. Curing Kinetics and Mechanical Properties of endo-Dicyclopentadiene Synthesized Using Different Grubbs' Catalysts. Industrial & Engineering Chemistry Research. 2014;53(8):3001-11.

16. Jones AS, Rule JD, Moore JS, White SR, Sottos NR. Catalyst morphology and

dissolution kinetics of self-healing polymers. Chemistry of Materials. 2006;18(5):1312-7.

17. Cui H, Kessler MR. Glass fiber reinforced ROMP-based bio-renewable polymers: enhancement of the interface with silane coupling agents. Composites Science and Technology. 2012;72(11):1264-72.

18. Sage Jr DB. Polyolefin fiber-reinforced composites using a fiber coating composition compatible with romp catalysts. Google Patents; 2002.

19. Yang G, Lee SC, Lee JK. Reinforcement of norbornene-based nanocomposites with norbornene functionalized multi-walled carbon nanotubes. Chemical Engineering Journal. 2016;288:9-18.

20. Becker EB, Carey GF, Oden JT. Finite elements: mathematical aspects: Prentice Hall; 1983.

21. Reddy JN, Gartling DK. The finite element method in heat transfer and fluid dynamics: CRC press; 2010.

22. Schlichting H, Gersten K, Krause E, Oertel H, Mayes K. Boundary-layer theory: Springer; 1960.

23. Currie IG. Fundamental mechanics of fluids: CRC Press; 2012.

24. Darcy H. Les fontaines publiques de la ville de Dijon: exposition et application: Victor Dalmont; 1856.

Figures

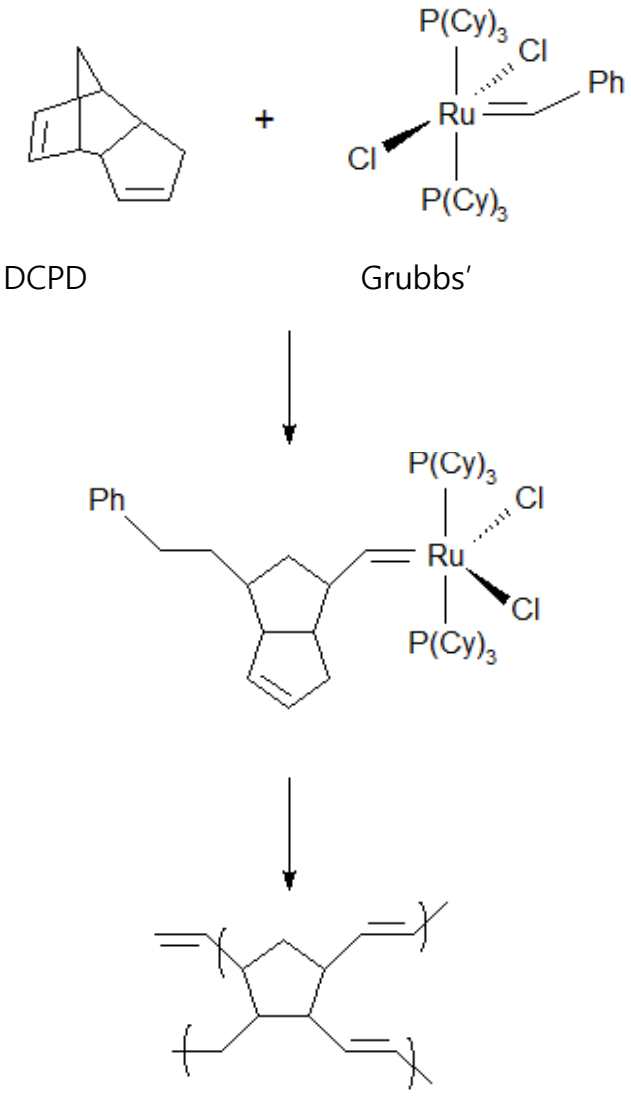

Figure 1 ROMP reaction mechanism.

Figure 2 Applications of p-DCPD.

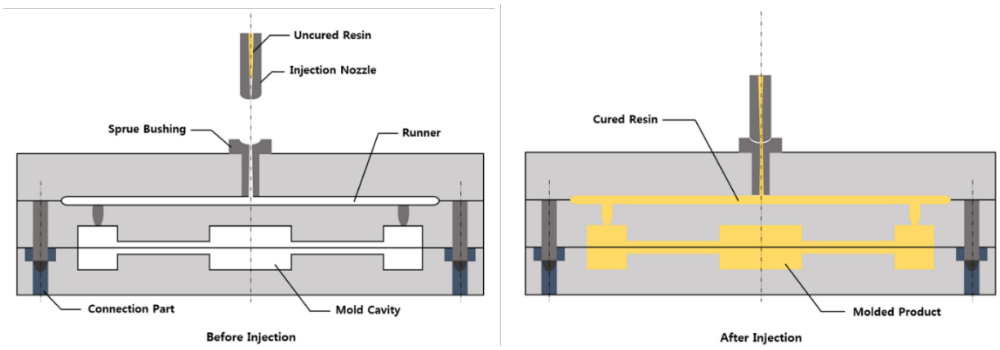

Figure 3 Reaction Injection Molding process

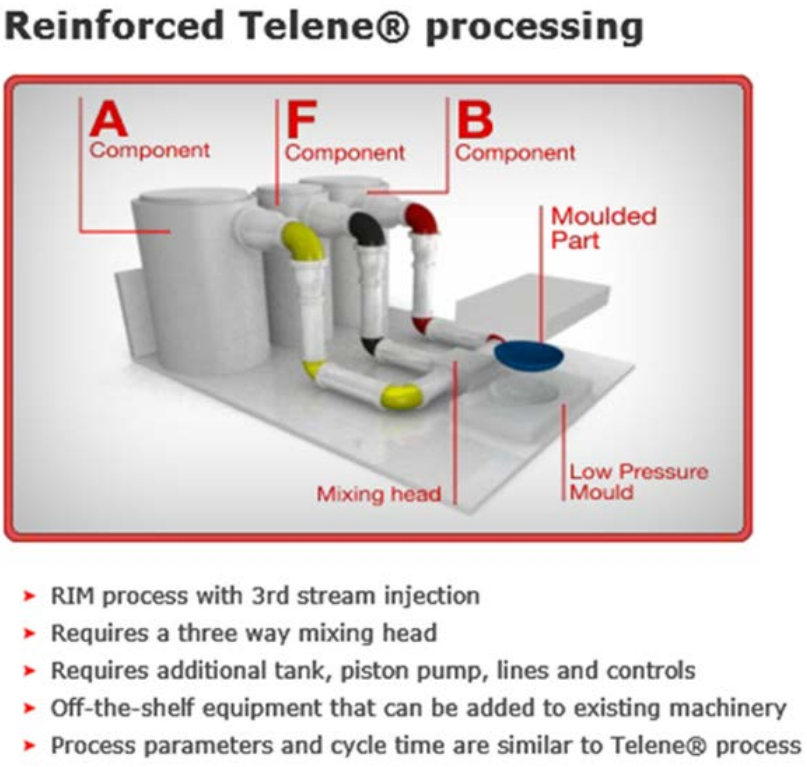

Figure 4 Reinforced reaction injection molding (R-RIM) process.

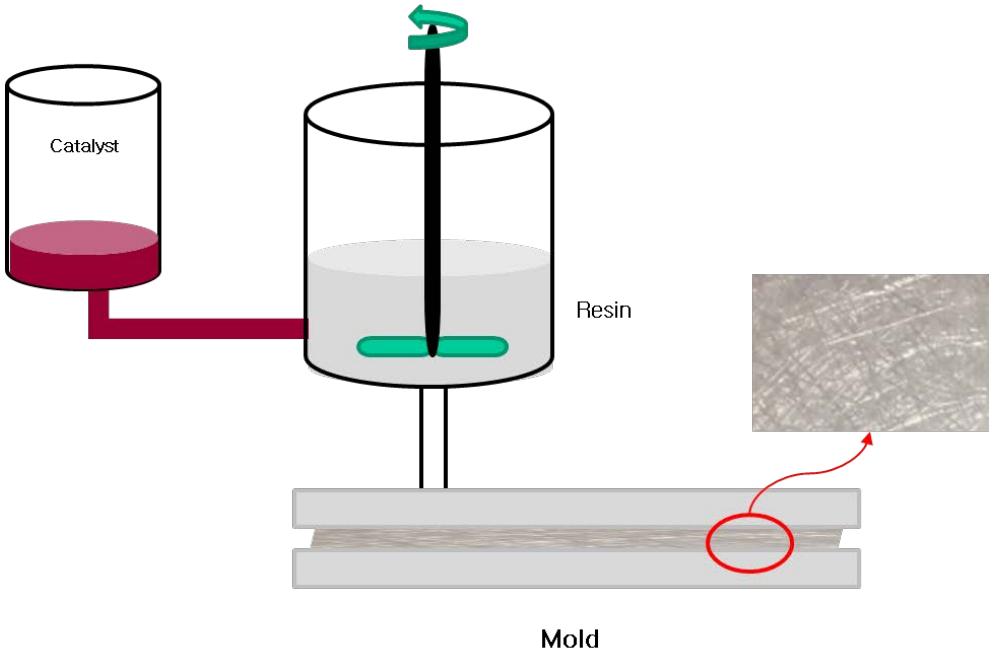

Figure 5 Structural reaction injection molding (S-RIM) process.

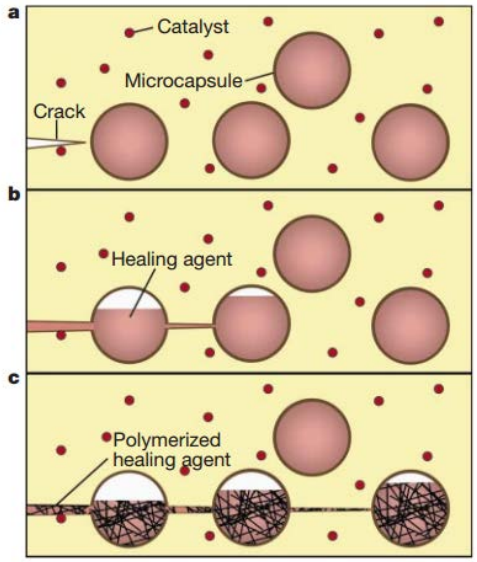

Figure 6 The autonomic healing concept, a microencapsulated healing agent is embedded in a structural composite matrix containing a catalyst capable of polymerizing the healing agent.

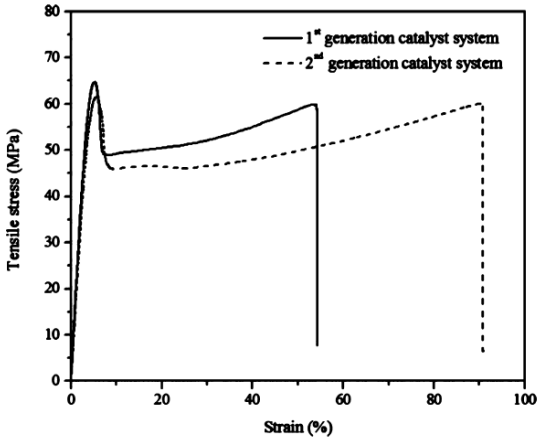

Figure 7 Stress-strain curves for poly-DCPD initiated by the first and second generation Grubbs' catalysts.

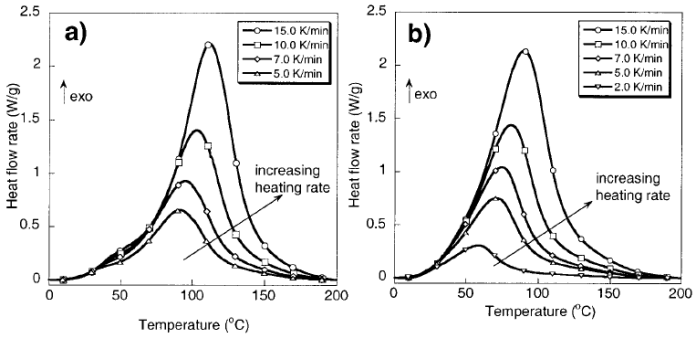

Concentration	Heating Rate (°C/min)	Sample Size Initial (mg)	Sample Size Final (mg)	Total Enthalpy of Reaction (J/g)
Low	15	9.3	8.9	456.7
	10	10.3	9.8	459.9
	7	8.3	8.1	453.5
	5	7.8	7.4	443.5
Medium	15	9.1	8.9	463.8
	10	6.3	6.1	457.3
	7	7.2	7.1	461.6
	5	11.6	11.3	478.8
	2	12.6	12.3	436.8
High	15	11.2	11.2	472.6
	10	10.8	10.7	485.3
	7	11.9	11.9	474.1
	5	11.1	11.1	467.5
	2	10.3	10.2	442.6

Figure 8 Curing kinetics of DCPD according to catalyst concentration and heating rate by DSC dynamic scanning results.

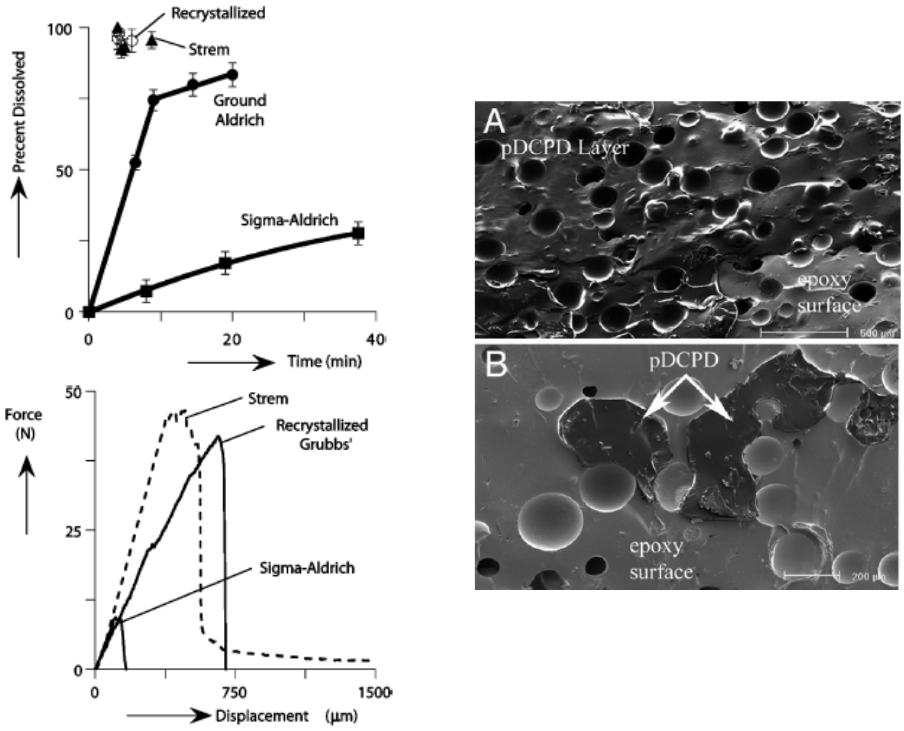

Figure 9 Catalyst morphology and dissolution kinetics of self-healing polymers. ESEM images of fracture surface showing (A) a continuous p-DCPD layer from a recrystallized catalyst specimen and (B) partial p-DCPD coverage from a Sigma-Aldrich catalyst specimen.

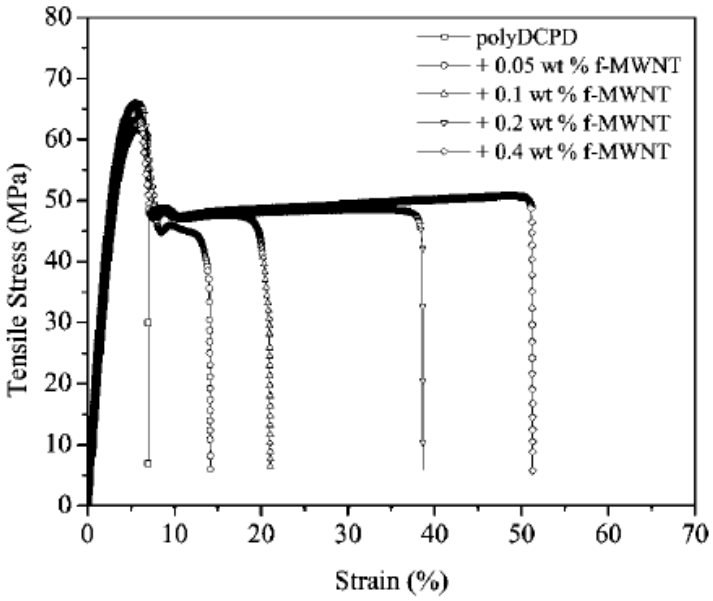

Figure 10 Stress-strain curves for norbonene-functionalized MWNT/pDCPD composites.

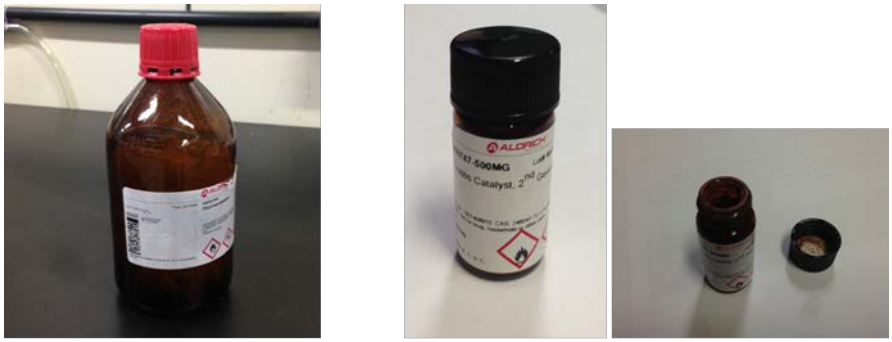

Figure 11 (a) Sigma-Aldrich's DCPD and (b) Grubbs catalyst.

Catalyst type	Tungsten(W) based catalyst	Molybdenum(Mo) based catalyst	Ruthenium(Ru) based catalyst
			
Component	TO2 A : DCPD + Catalyst TO2 B : DCPD + Activator	Telene 1690A : DCPD + Catalyst Telene 1690B : DCPD + Activator Telene 1690F : DCPD monomer	Ru catalyst : Grubbs 2nd catalyst
Supplier	RIMTEC Corp.	RIMTEC Corp.	RIMTEC Corp. Sigma-Aldrich Corp.
Mixing ratio	A:B = 1:1	A:B:F = 1:1:1	MS:Cat. = 1:0.002

Figure 12 A type of RIMTEC's DCPD resin.

Type	Milled glass fiber & Chopped glass fiber	Chopped glass strand mat	Carbon woven fabric
		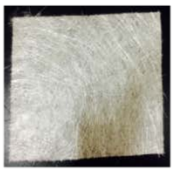	
Model	737BD, 123D (D : 10 μm)	M723 (380g/m^2, 450g/m^2)	C-120 (3K)
Length	100μm, 4mm	50mm	Continuous
Supplier	Owens corning Corp.	Owens corning Corp.	Muhan composite

Figure 13 A type of reinforcement

Catalyst type	Tungsten(W) based catalyst	Molybdenum(Mo) based catalyst	Ruthenium(Ru) based catalyst
			
Component	TO2 A : DCPD + Catalyst TO2 B : DCPD + Activator	Telene 1690A : DCPD + Catalyst Telene 1690B : DCPD + Activator Telene 1690F : DCPD monomer	Ru catalyst : Grubbs 2nd catalyst
Density	1.03 g/cm^3.	1.03 g/cm^3.	0.986 g/cm^3
Viscosity	0.4 pa·s	0.4 pa·s	< 0.1pa·s

Figure 14 Density and viscosity of DCPD resins.

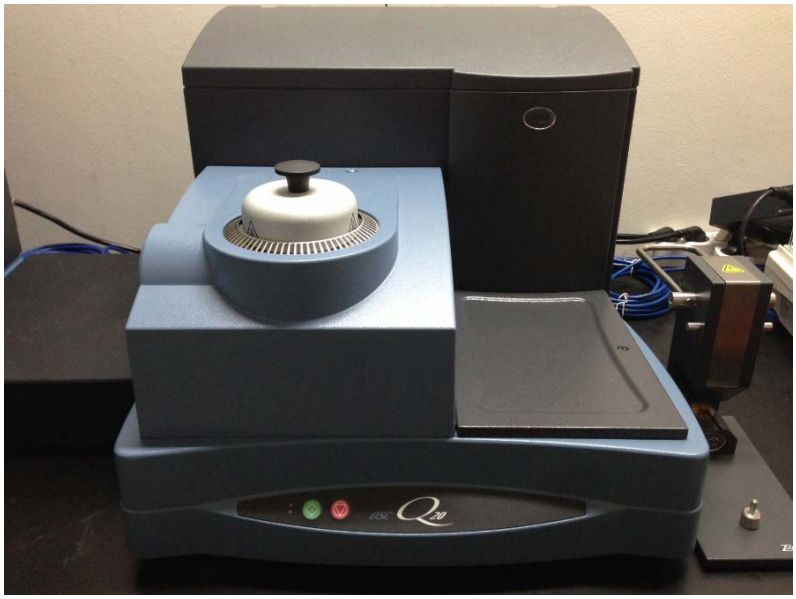

Figure 15 DSC (Q20, TA Instrument).

Figure 16 Liquid nitrogen.

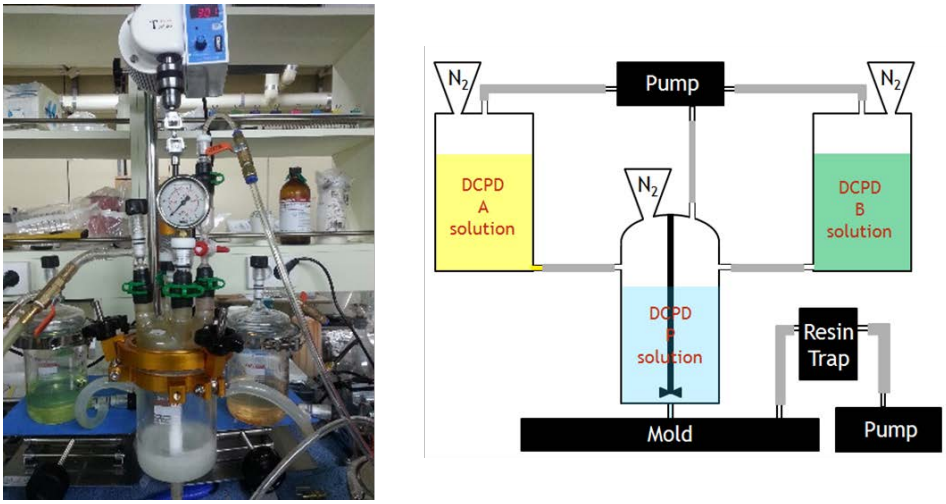

Figure 17 Schematic diagram of R-RIM equipment.

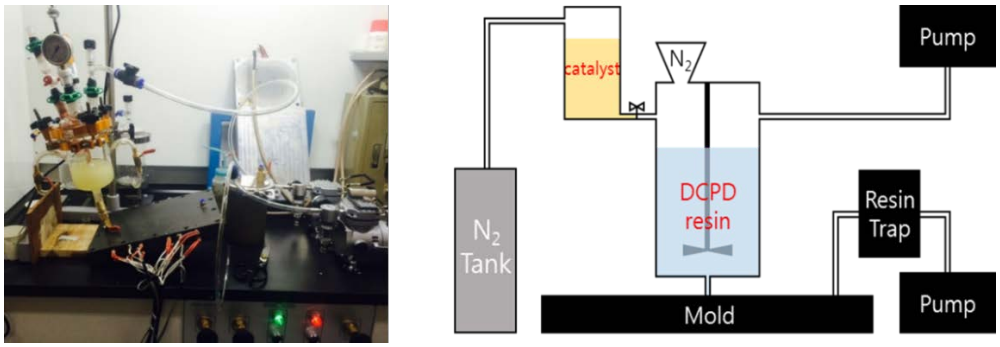

Figure 18 Schematic diagram of S-RIM equipment.

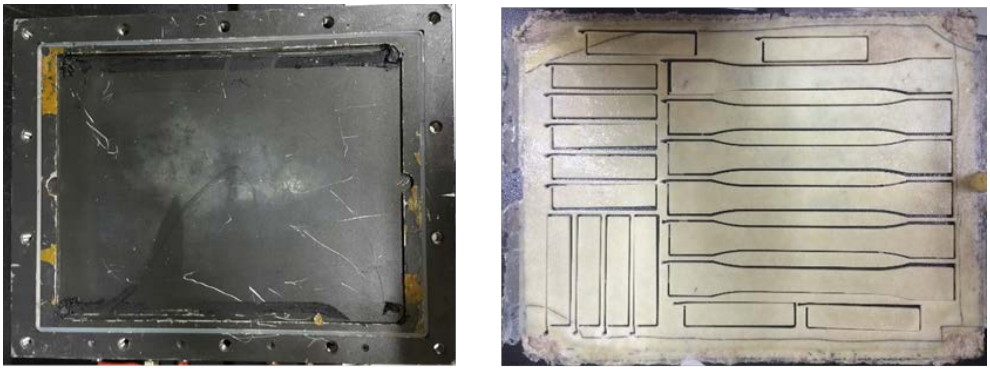

(a) (b)

Figure 19 Mold (a) and manufactured compostie specimen (b)

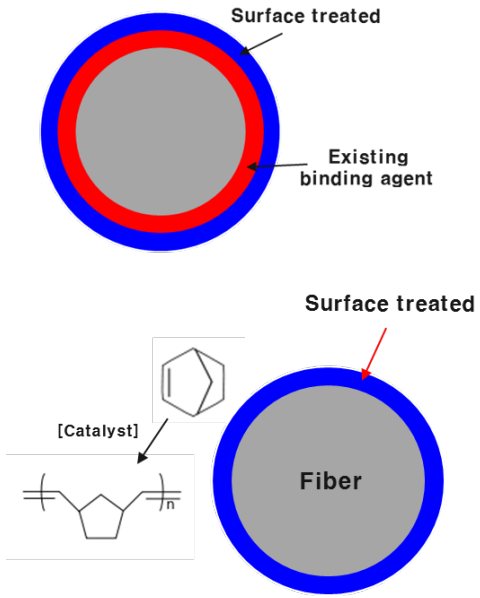

Figure 20 Surface treatment using norbornene based silane.

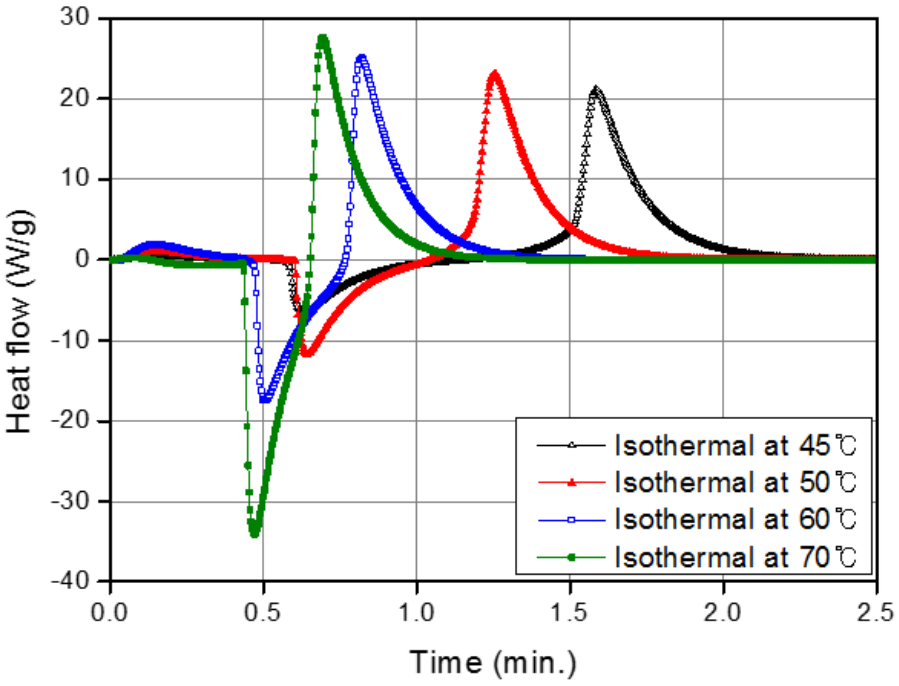

Figure 21 DSC results with different isothermal temperature.

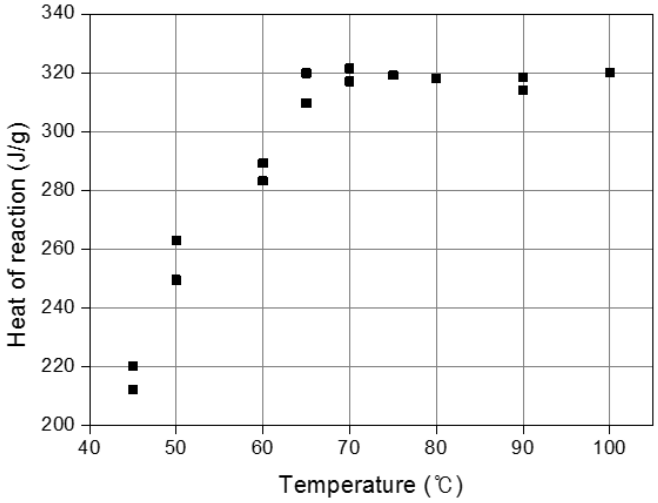

Figure 22 Total heat of reaction of DCPD at different temperatures.

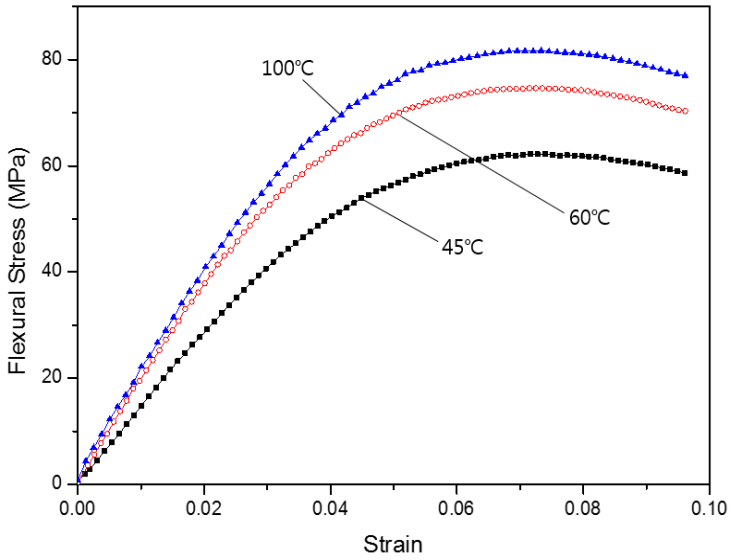

Figure 23 Three point bending test.

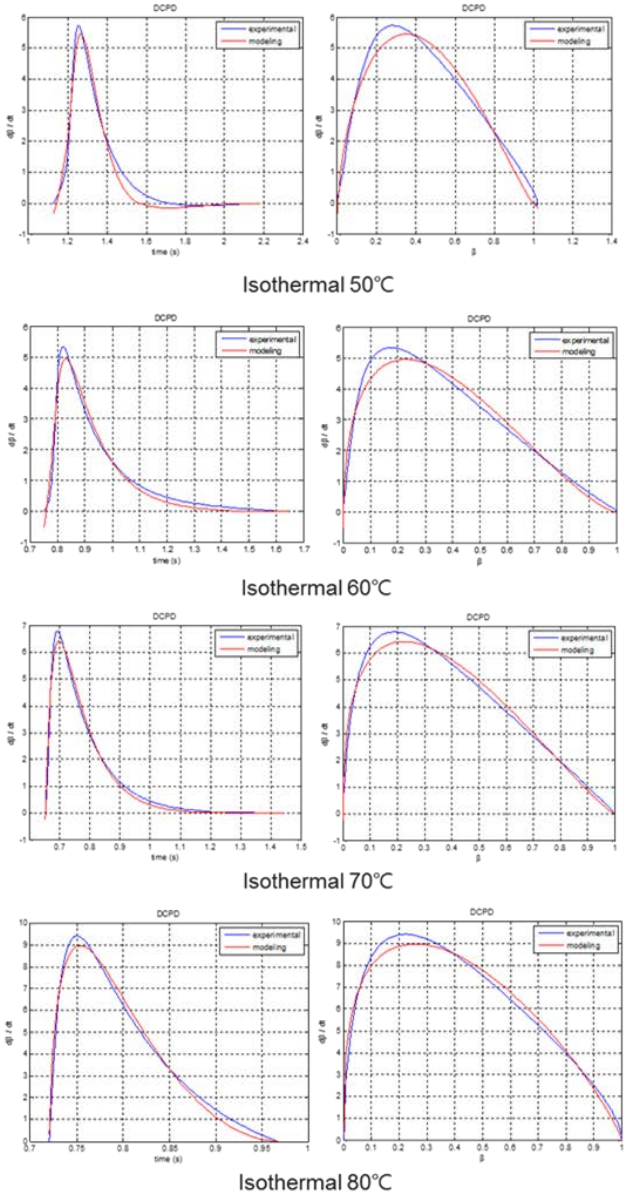

Figure 24 curing kinetics of DCPD using autocatalytic model.

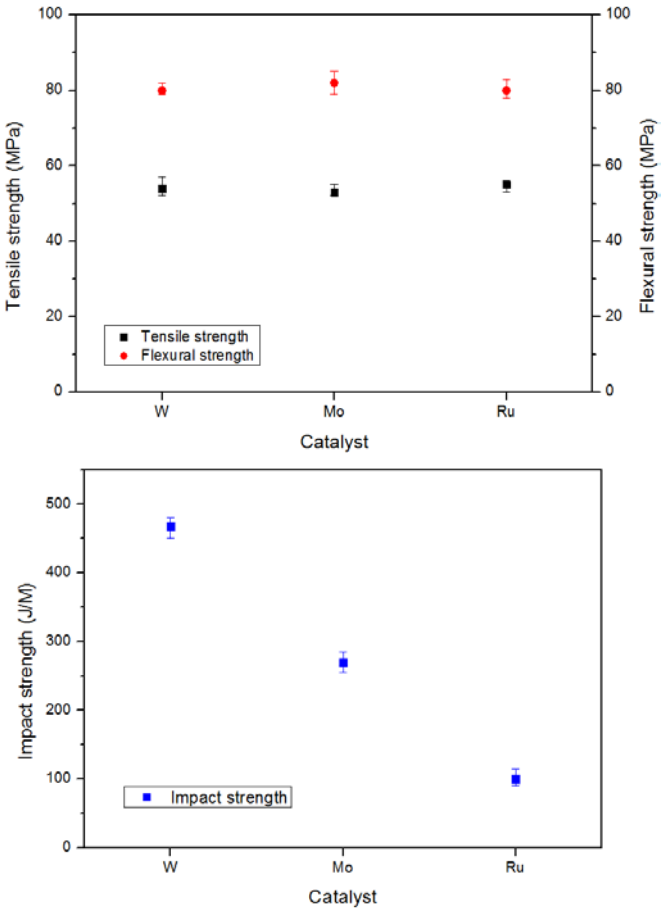

Figure 25 Mechanical properties of p-DCPD for different catalsyts.

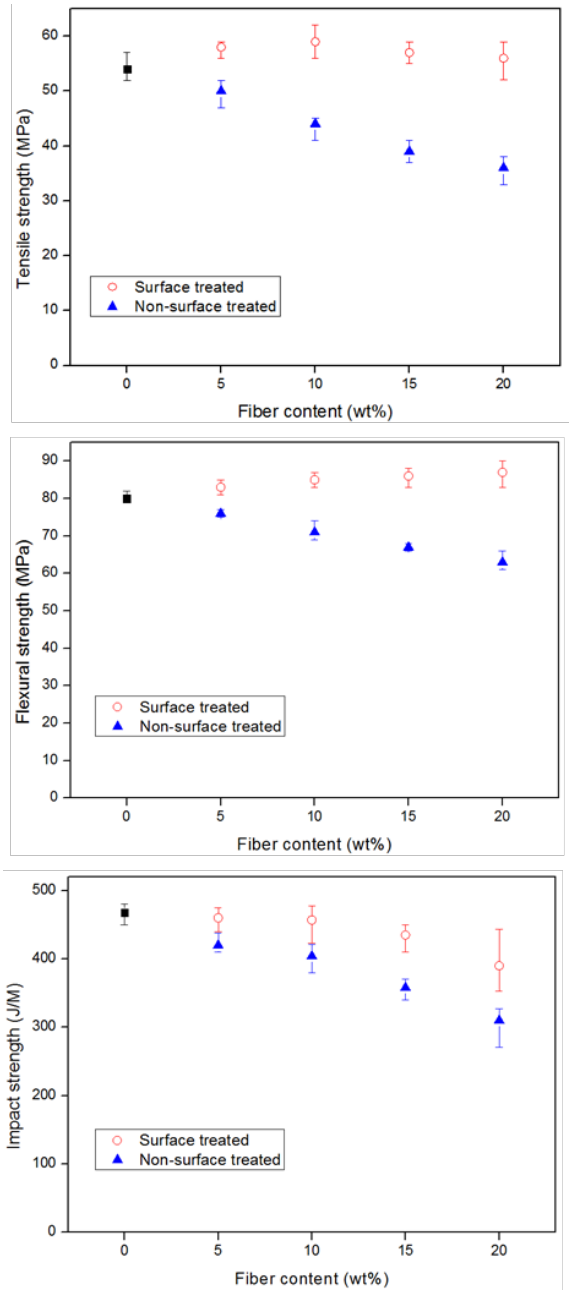

Figure 26 Mechanical properties of GF/p-DCPD composites (W based catalyst).

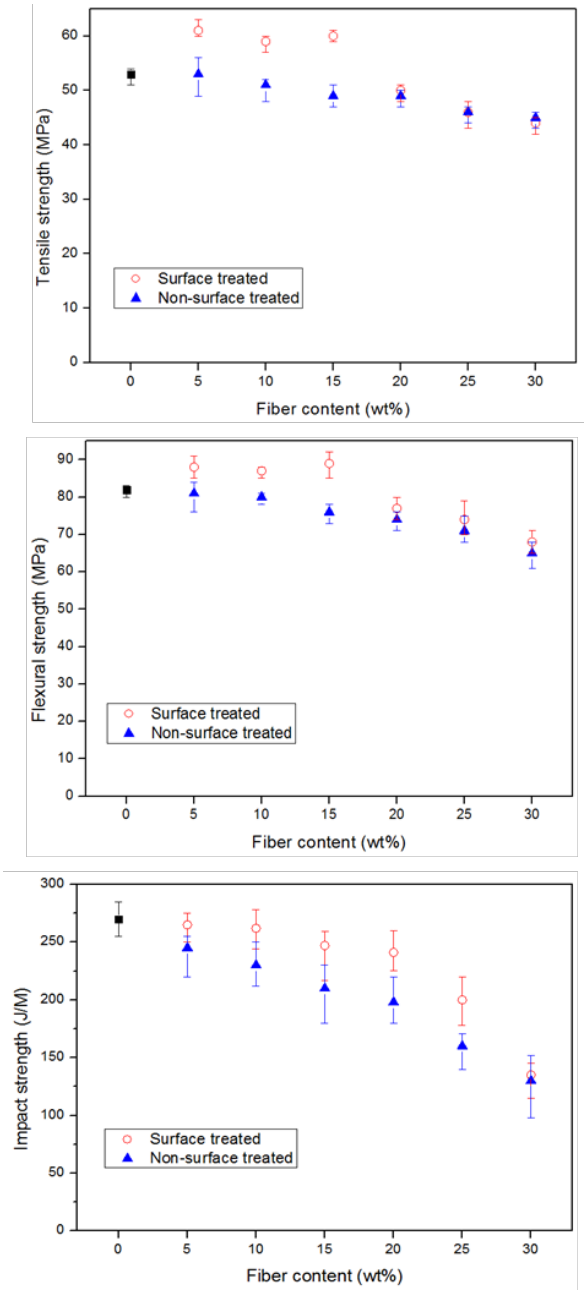

Figure 27 Mechanical properties of GF/p-DCPD composites (Mo based catalyst).

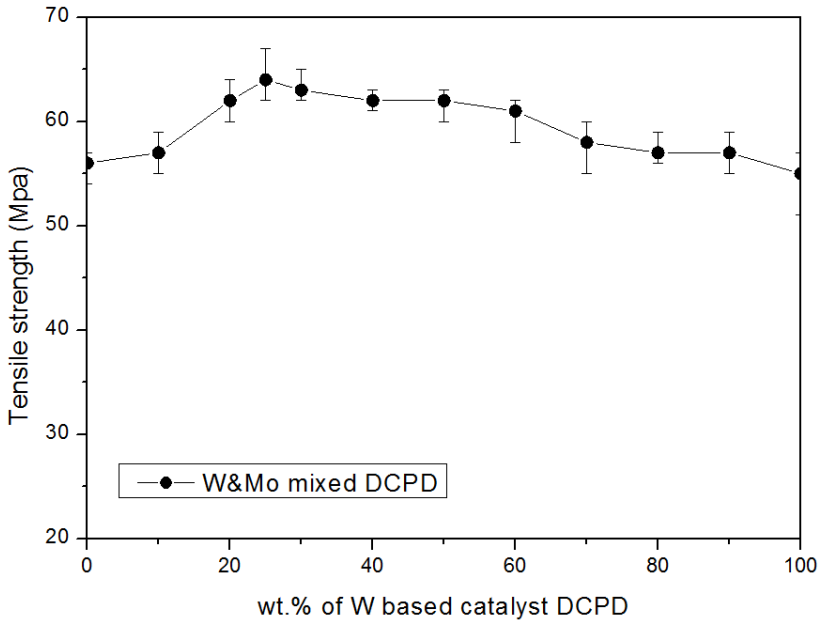

Figure 28 Tensile strengths of p-DCPD using mixed catalyst (W, Mo based catalyst).

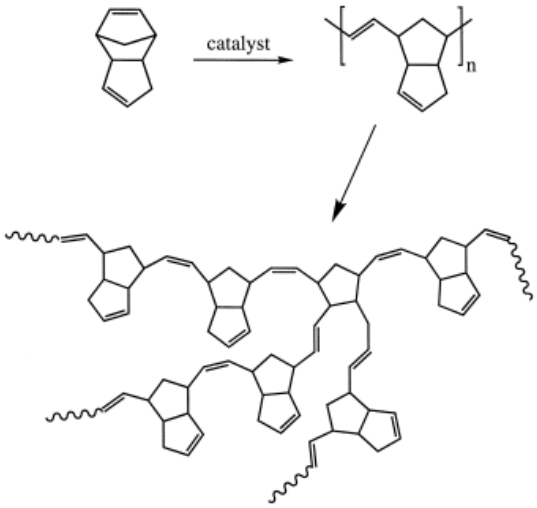

Figure 29 ROMP mechanism of dicyclopentadiene.

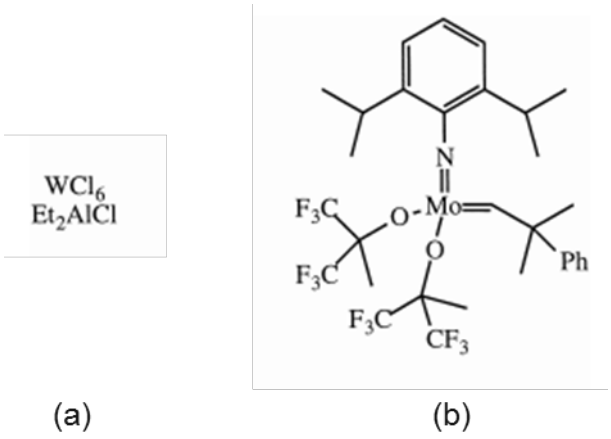

Figure 30 Molecular structure of W based catalyst(a) and Mo based catalyst(b).

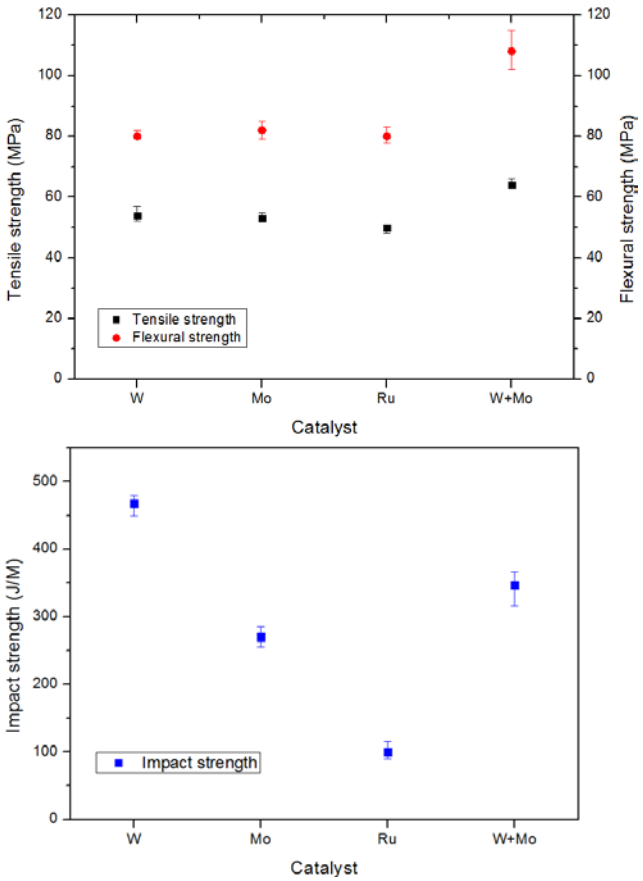

Figure 31 Mechanical properties of p-DCPD using different catalsyts (added the mixed catalsyt).

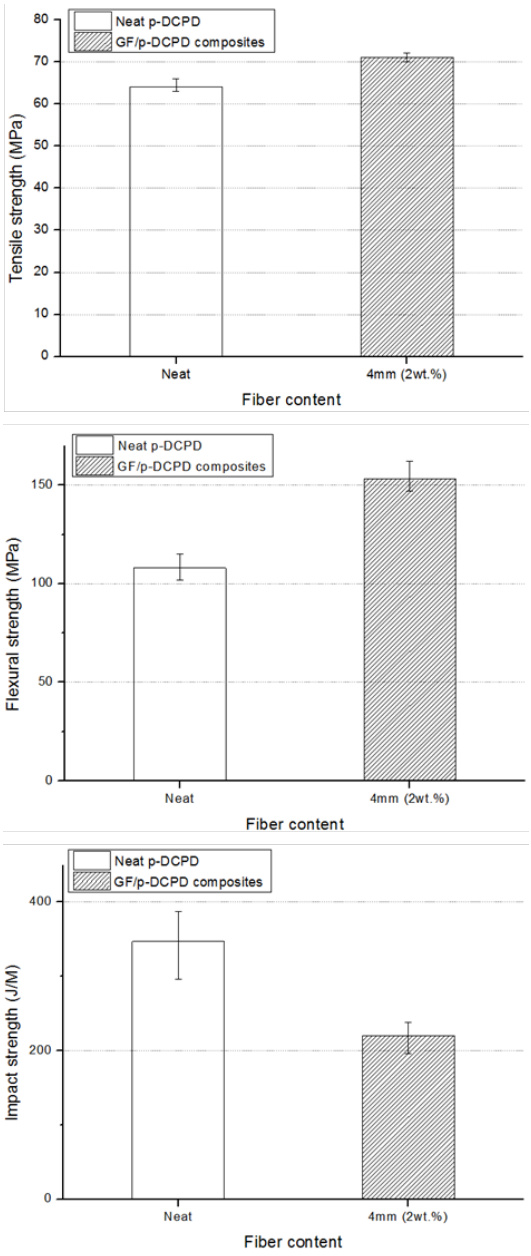

Figure 32 Mechanical properties of GF/p-DCPD composites (W+Mo based catalyst, 4mm Chopped glass fiber).

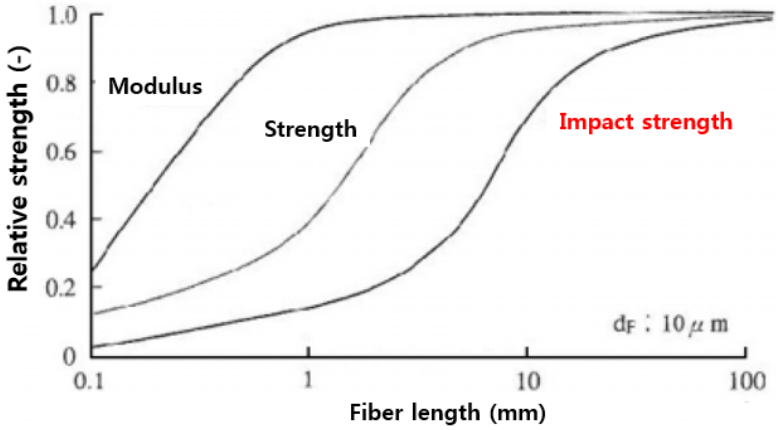

Figure 33 Mechanical properties change according to the fiber length.

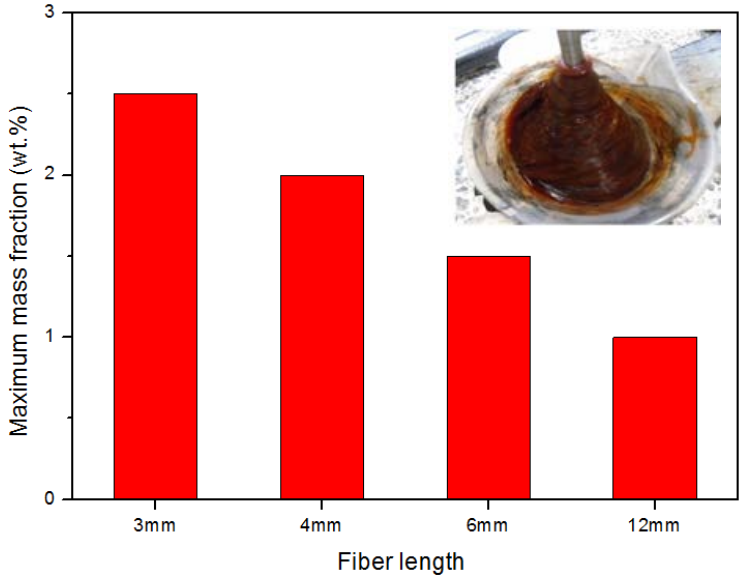

Figure 34 Maximum amount of fiber that can be added.

Figure 35 S-RIM process using mixed catalsyt (W, Mo).

Figure 36 Specimen of GF/p-DCPD composites manufactured by S-RIM.

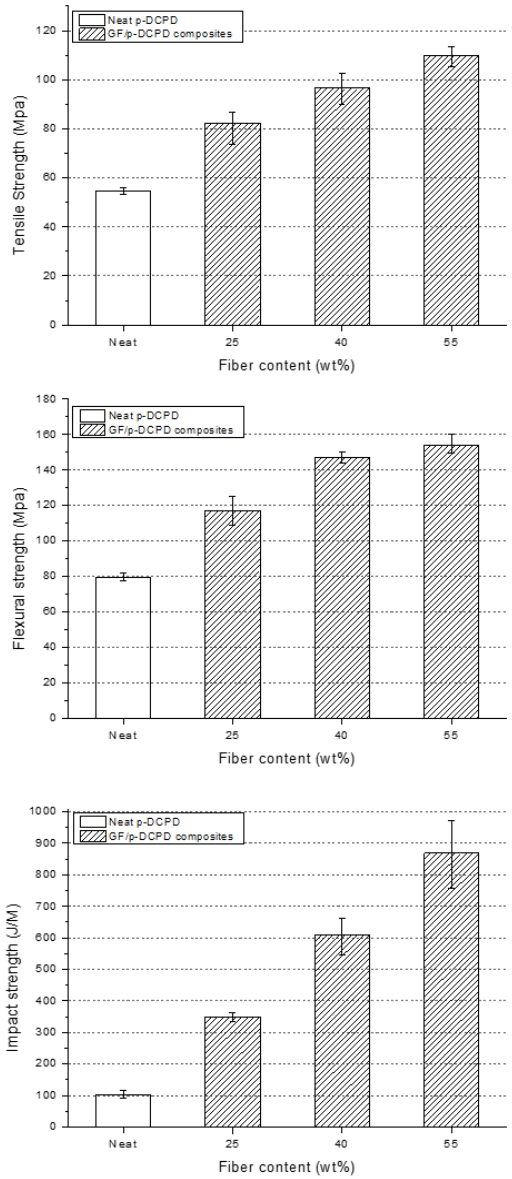

Figure 37 Mechanical properties of GF/p-DCPD composites manufactured by S-RIM (Ru based catalsyt).

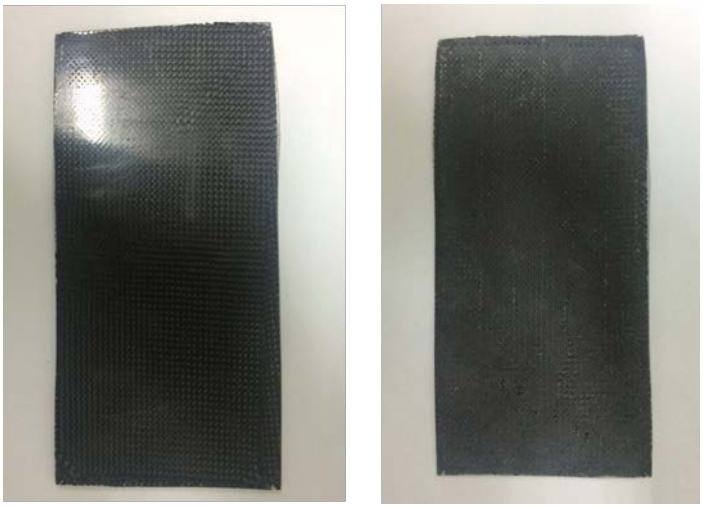

Figure 38 CF/p-DCPD composite specimen.

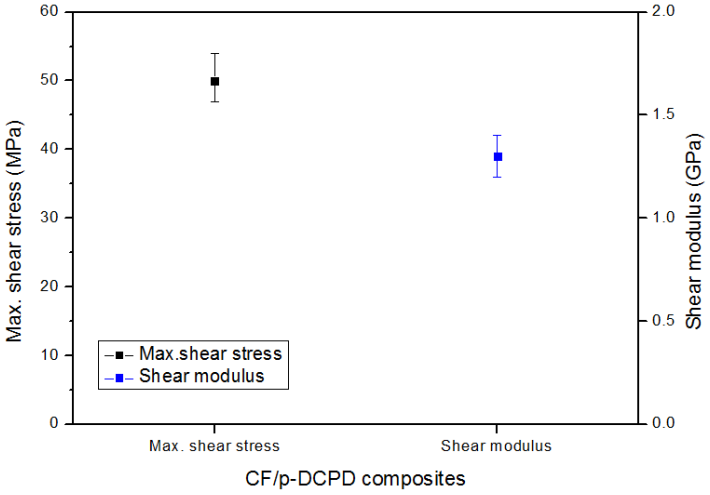

Figure 39 Max. shear stress and shear modulus of CF/p-DCPD composites.

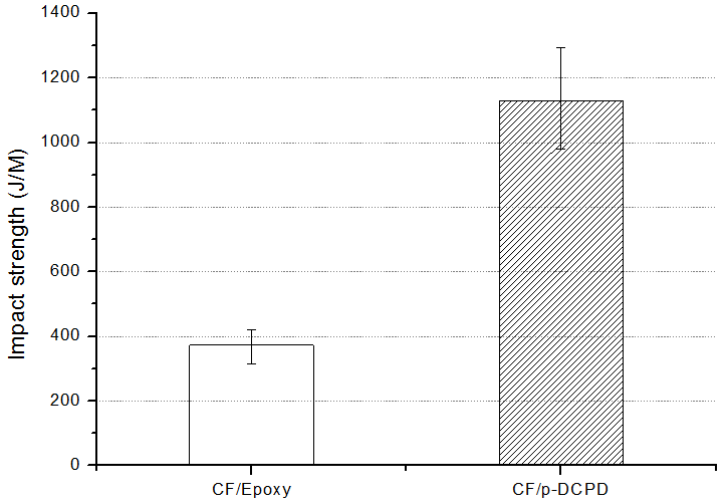

Figure 40 Impact strength of CF/Epoxy and CF/p-DCPD composites.

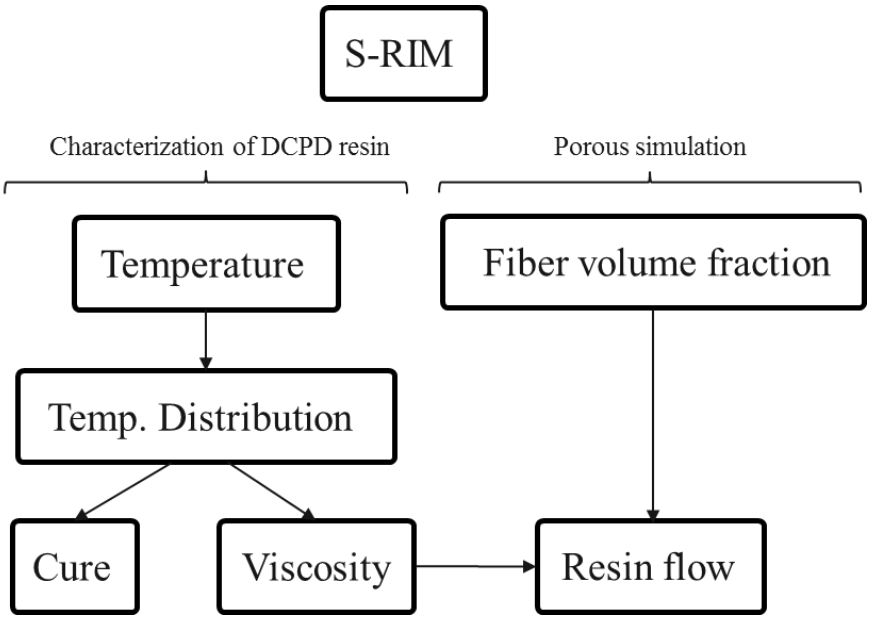

Figure 41 Modeling process of fiber reinforced DCPD composites.

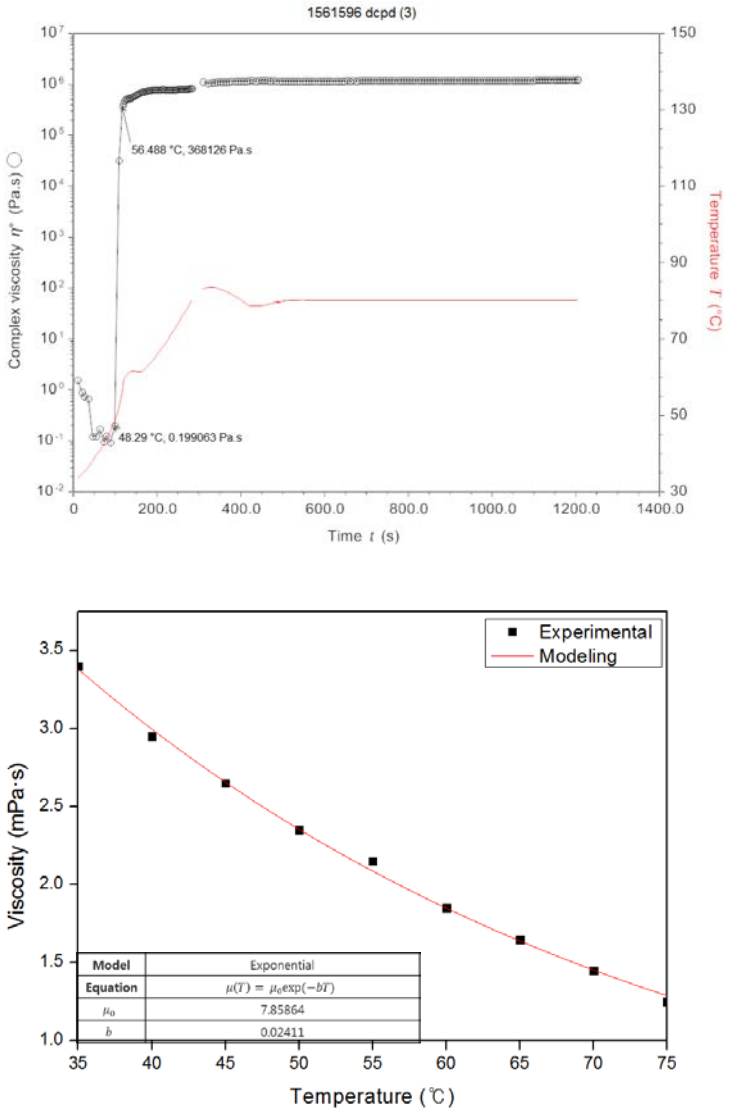

Figure 42 Viscosity change with temperature using exponential viscosity model.

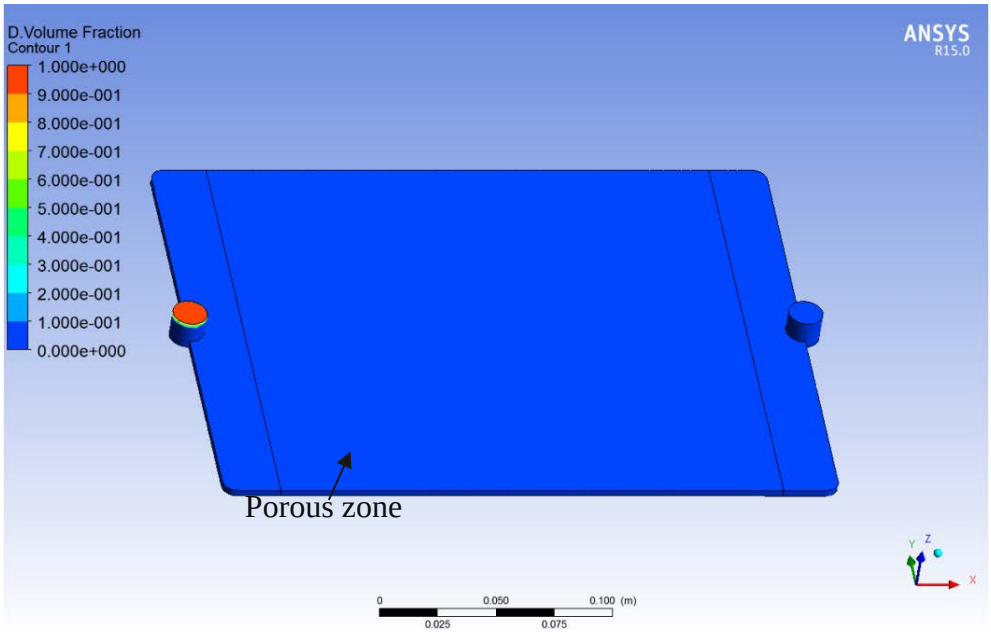

Figure 43 Geometry about numerical simulation of DCPD resin flow with porous zone.

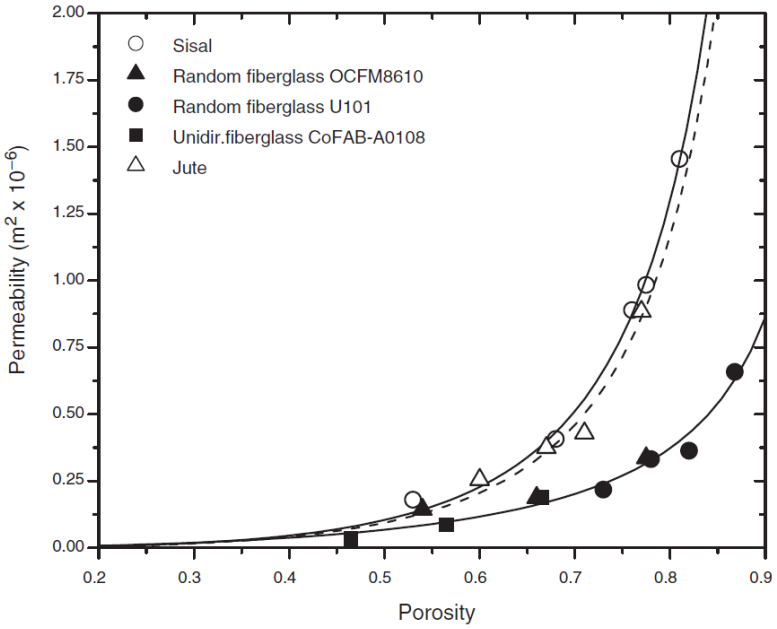

Figure 44 Permeability-porosity relationship in RTM for random fiber glass.

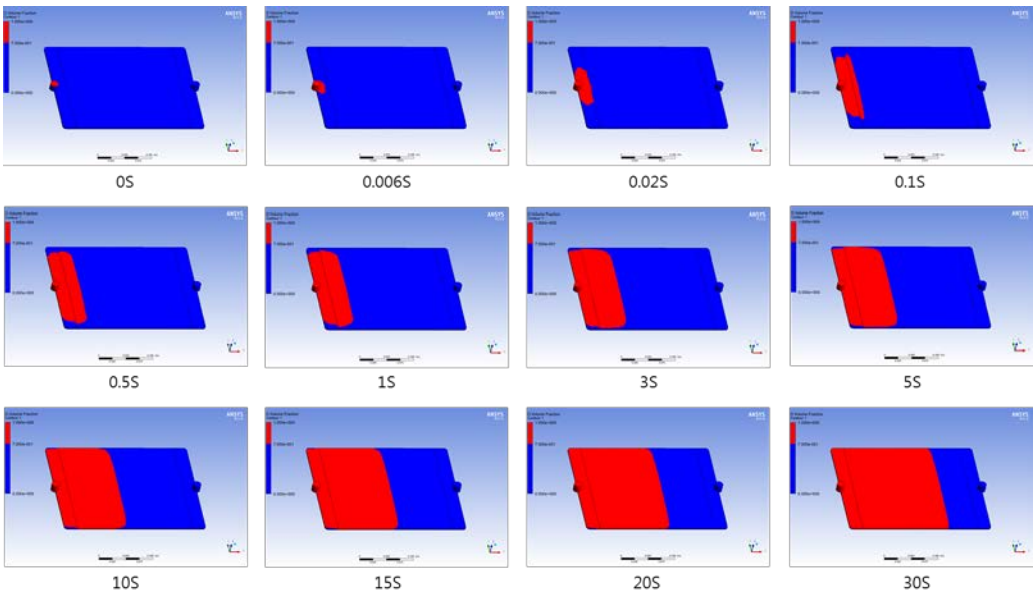

Figure 45 Numerical simulation of DCPD resin flow (at 0.4pa·s).

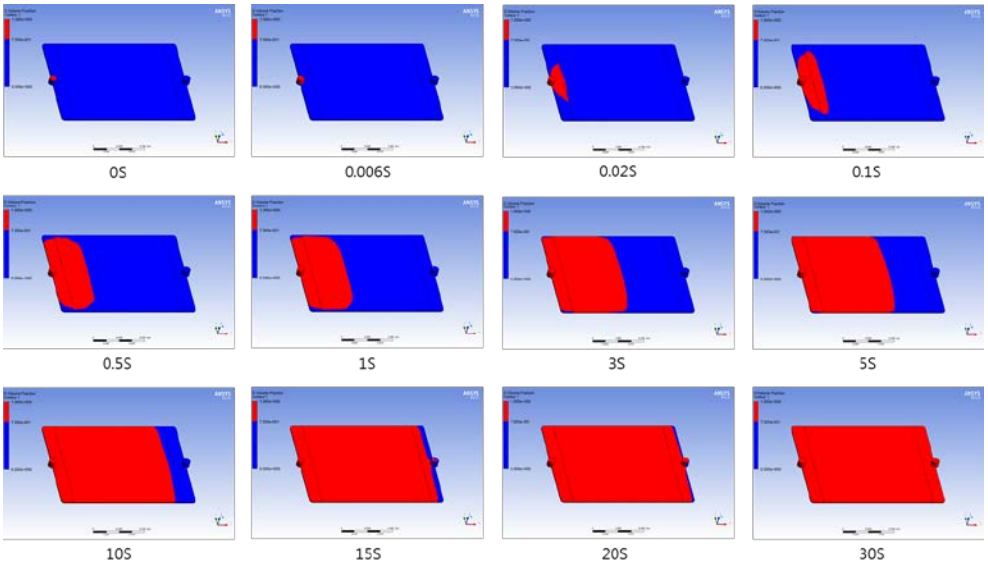

Figure 46 Numerical simulation of DCPD resin flow (at 0.1pa·s).

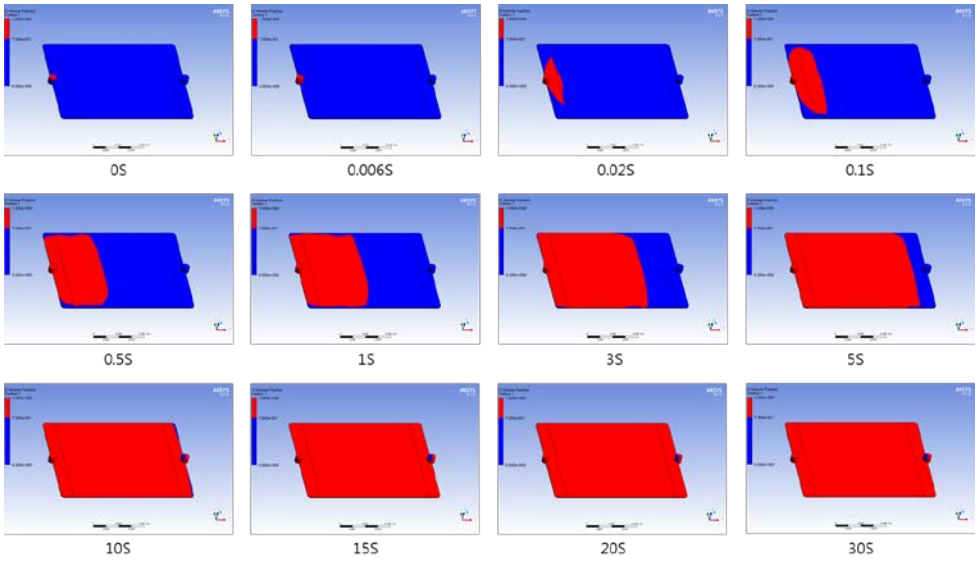

Figure 47 Numerical simulation of DCPD resin flow (at 0.04pa·s).

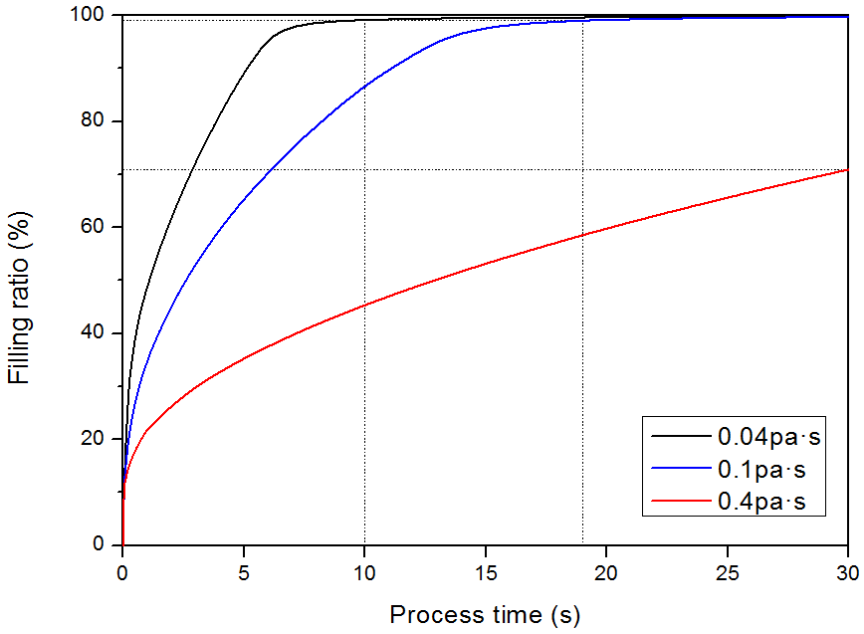

Figure 48 Filling ratio for different resin viscosity.

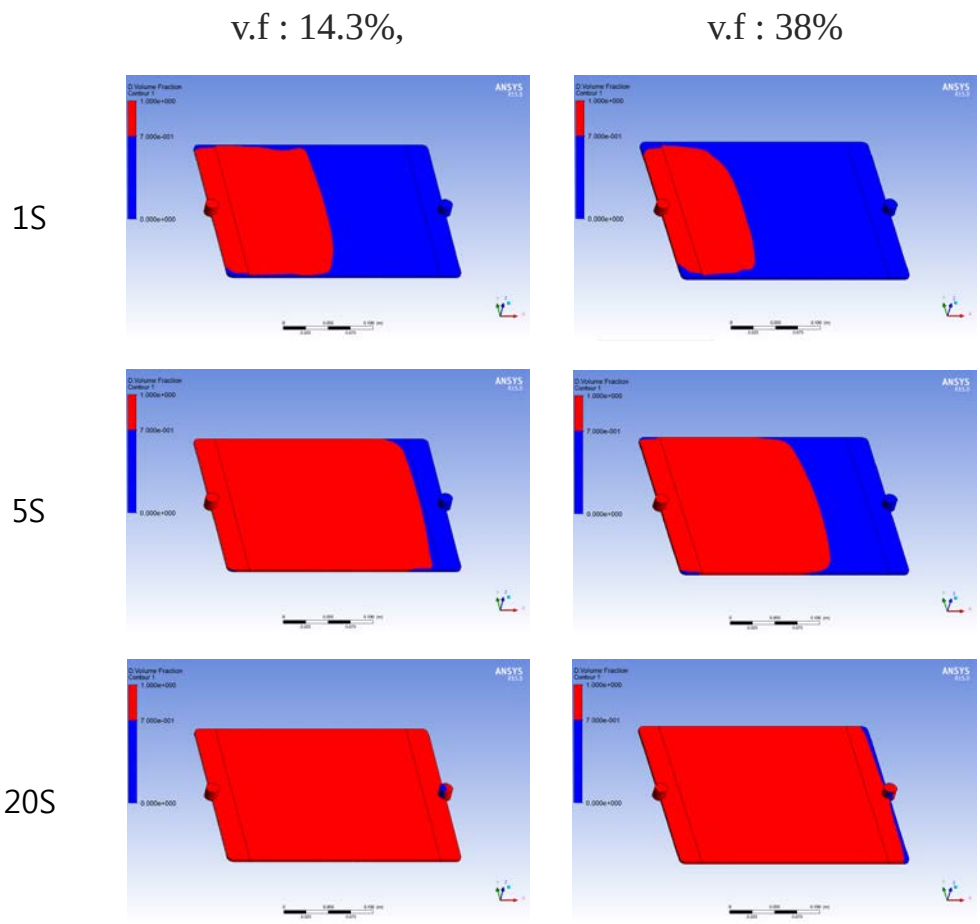

Figure 49 Numerical simulation of DCPD resin flow for different fiber volume fraction.

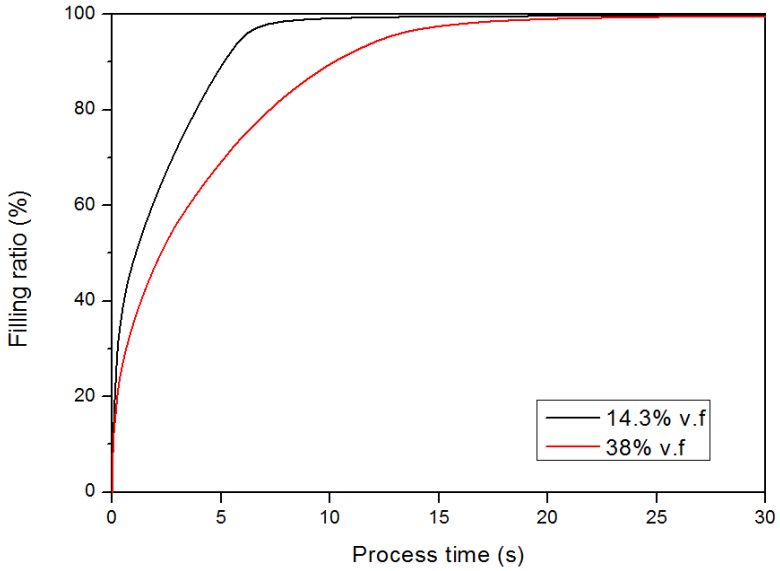

Figure 50 Filling ratio for different fiber volume fraction.

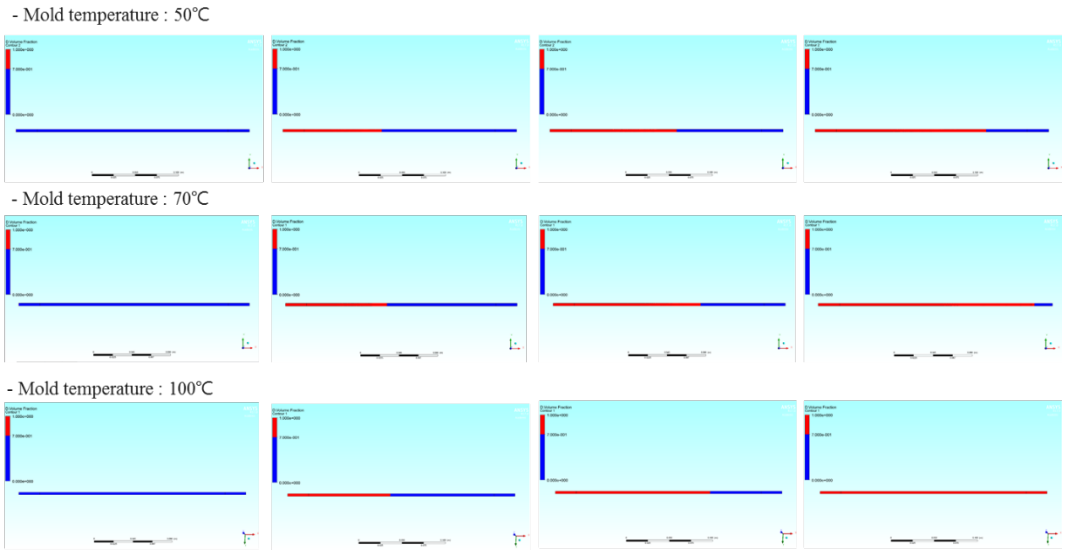

Figure 51 Numerical simulation of DCPD resin flow for different mold temperature.

- Mold temperature : 50℃

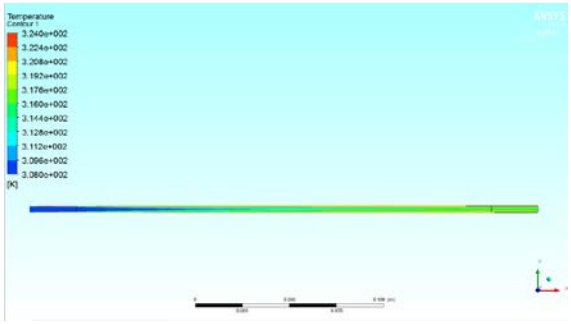

- Mold temperature : 70℃

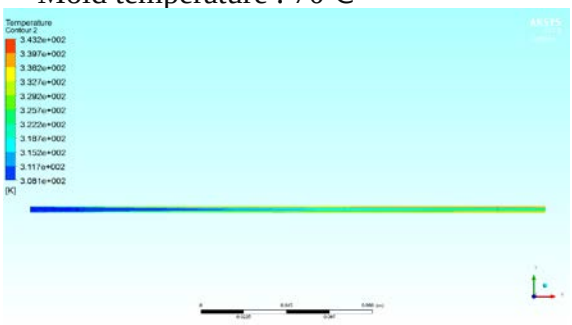

- Mold temperature : 100℃

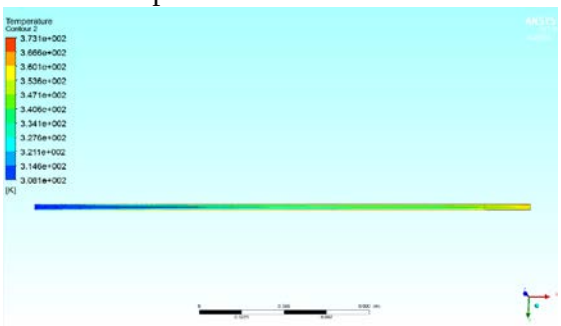

Figure 52 Temperature distribution of resin with mold temperature.

Tables

Table 1 Three point bending test results of p-DCPD by different curing temperatures.

Sample	Temperature (℃)	σ_f (MPa)	E_B (GPa)
Poly-DCPD	45	63±1.8	1.5±0.04
	60	75±0.6	1.8±0.03
	100	79±1.7	1.9±0.07

Table 2 Coefficient calculation of autocatalytic model.

	50℃	**60℃**	**70℃**	**80℃**
K_1**(T)**	1.25	1.04	1.23	1.09
K_2**(T)**	14.3	14.0	15.7	17.4
M	0.41			
n	1.22			

Table 3 Comparing tensile properties of specimen using closed and open mold.

	Ultimate strength(Mpa)	Elastic modulus(Gpa)
Closed mold	52.75	0.84
Open mold	39.9	0.73

Table 4 Mechanical properties of p-DCPD using different catalysts.

Sample	Catalyst	Tensile strength (MPa)	Flexural strength (MPa)	Impact strength (J/M)
p-DCPD	W	54	80	468
	Mo	53	82	270
	Ru	55	80	100

Table 5 Mechanical properties of GF/p-DCPD composites manufactured by S-RIM (Ru based catalsyt).

Sample	Fiber content (wt.%)	Tensile strength (MPa)	Flexural strength (MPa)	Impact strength (J/M)
Poly-DCPD	Neat	54.8±1.1	79.4±1.7	100.2±10
GF/p-DPCD	25	82±5.8	120±12.1	349±11
composites	40	96.5±4.7	147±2.1	609±56
	55	110±3.7	153±4.5	869±94

Table 6 Max. shear stress and shear modulus of CF/p-DCPD composites.

Sample	Fiber content (wt.%)	Max. Shear stress (MPa)	Shear modulus (GPa)
CF/p-DCPD composites	55	50	1.3

디사이클로펜타디엔 수지를 이용한 복합재료 액상성형공정 모델링 및 최적화

서울대학교 대학원

기계항공공학부

유 형 민

요약(국문초록)

경량화를 위한 복합재료가 군수분야 뿐만 아니라 민수분야에 적용됨에 따라 내충격성 향상을 통한 안정성 증대와 생산비용을 절감하려는 노력이 이루어지고 있다. 디사이클로펜타디엔 수지는 낮은 점성의 무색액체로 촉매와 반응하여 짧은 시간 안에 복분해중합반응이 일어나 그물구조의 폴리디사이클로펜타이엔을 형성하는데, 이렇게 형성된 폴리디사이클로펜타디엔은 내한성, 내수성 및 내충격성이 우수한 특성을 가진다. 낮은 점도를 가지는 수지 특성을 이용하여 액상성형을 통한 제품 개발 연구가 진행되고 있으나 모노머 특유의 경화반응, 대기중의 반응 불안정성 등의 이유로 강화재를 첨가한 디사이클로펜타디엔 성형공정에 관한 연구가 부족하다. 본 연구에서는 디사이클로펜타디엔 수지의 경화특성을 시차주사열량측정법으로 분석, 모델링하고

그 결과를 토대로 강화재 첨가 가능한 액상성형장비를 설계하였다. 섬유의 부피분율, 길이에 따라 두 가지 액상성형방법으로 장비를 구축하였으며 이를 이용한 시편을 제작, 기계적 물성 평가를 진행하였다. 또한 수치해석 수행을 통해 복합재료 액상성형공정에서 수지의 점도, 섬유의 부피분율에 따라 공정시간을 예측하였고 그에 적합한 액상성형공정을 제시하였으며 액상성형공정에서 공정 온도, 섬유의 부피분율 등의 공정 변수를 설정하고 이를 이용한 최적화를 통해 섬유 강화 디사이클로펜타디엔 수지 복합재료를 제작할 수 있음을 보였다.

주요어 : 디사이클로펜타디엔, 강화섬유, 액상성형공정, 시차주사열량측정법

학번 : 2012 – 22559